TU Delft

Delft University of Technology

Wave-Driven Hydrodynamic Processes Over Fringing Reefs With Varying Slopes, Depths, and Roughness

Implications for Coastal Protection

Buckley, Mark L.; Lowe, Ryan J.; Hansen, Jeff E.; van Dongeren, Ap R.; Pomeroy, Andrew; Storlazzi, Curt D.; Rijnsdorp, Dirk P.; da Silva, Renan F.; Contardo, Stephanie; Green, Rebecca H.

DOI
10.1029/2022JC018857

Publication date
2022

Document Version
Final published version

Published in
Journal of Geophysical Research: Oceans

Citation (APA)
Buckley, M. L., Lowe, R. J., Hansen, J. E., van Dongeren, A. R., Pomeroy, A., Storlazzi, C. D., Rijnsdorp, D. P., da Silva, R. F., Contardo, S., & Green, R. H. (2022). Wave-Driven Hydrodynamic Processes Over Fringing Reefs With Varying Slopes, Depths, and Roughness: Implications for Coastal Protection. *Journal of Geophysical Research: Oceans*, *127*(11), Article e2022JC018857. https://doi.org/10.1029/2022JC018857

Important note
To cite this publication, please use the final published version (if applicable).
Please check the document version above.

Copyright
Other than for strictly personal use, it is not permitted to download, forward or distribute the text or part of it, without the consent of the author(s) and/or copyright holder(s), unless the work is under an open content license such as Creative Commons.

Takedown policy
Please contact us and provide details if you believe this document breaches copyrights.
We will remove access to the work immediately and investigate your claim.

This work is downloaded from Delft University of Technology.
For technical reasons the number of authors shown on this cover page is limited to a maximum of 10.

Green Open Access added to TU Delft Institutional Repository

'You share, we take care!' - Taverne project

https://www.openaccess.nl/en/you-share-we-take-care

Otherwise as indicated in the copyright section: the publisher is the copyright holder of this work and the author uses the Dutch legislation to make this work public.

Check for updates

JGR Oceans

RESEARCH ARTICLE
10.1029/2022JC018857

Key Points:

- SWASH reproduced laboratory observations of waves and runup over both smooth and rough fringing reefs
- Fore-reef slope controls wave runup on reef-fringed coasts as opposed to beach slope on plane open coast beaches
- Wave runup was sensitive to bottom roughness with tall roughness elements on the reef flat generating the greatest runup reduction

Correspondence to:
M. L. Buckley,
mbuckley@usgs.gov

Citation:
Buckley, M. L., Lowe, R. J., Hansen, J. E., van Dongeren, A. R., Pomeroy, A., Storlazzi, C. D., et al. (2022). Wave-driven hydrodynamic processes over fringing reefs with varying slopes, depths, and roughness: Implications for coastal protection. *Journal of Geophysical Research: Oceans*, *127*, e2022JC018857. https://doi.org/10.1029/2022JC018857

Received 16 MAY 2022
Accepted 5 OCT 2022

© 2022 American Geophysical Union. All Rights Reserved. This article has been contributed to by U.S. Government employees and their work is in the public domain in the USA.

Wave-Driven Hydrodynamic Processes Over Fringing Reefs With Varying Slopes, Depths, and Roughness: Implications for Coastal Protection

Mark L. Buckley[1], Ryan J. Lowe[2], Jeff E. Hansen[2], Ap R. van Dongeren[3,4], Andrew Pomeroy[5], Curt D. Storlazzi[6], Dirk P. Rijnsdorp[7], Renan F. da Silva[2], Stephanie Contardo[2,8], and Rebecca H. Green[2]

[1]U.S. Geological Survey, St. Petersburg Coastal and Marine Science Center, St. Petersburg, FL, USA, [2]The University of Western Australia, Crawley, Australia, [3]Department ZKS, Deltares, Delft, The Netherlands, [4]Department CURR, IHE Delft, Delft, The Netherlands, [5]The University of Melbourne, Parkville, Australia, [6]U.S. Geological Survey, Pacific Coastal and Marine Science Center, Santa Cruz, CA, USA, [7]Environmental Fluid Mechanics Section, Faculty of Civil Engineering and Geosciences, Delft University of Technology, Delft, The Netherlands, [8]CSIRO Oceans and Atmosphere, Crawley, Australia

Abstract Wave breaking on the steep fore-reef slopes of shallow fringing reefs can be effective at dissipating incident sea-swell waves prior to reaching reef shorelines. However, wave setup and free infragravity waves generated during the sea-swell breaking process are often the largest contributors to wave-driven water levels (wave runup) at the shoreline. Laboratory flume experiments and a two-dimensional vertical phase-resolving nonhydrostatic wave-flow model, which includes a canopy model to predict drag forces generated by roughness elements, were used to investigate wave-driven water levels for along-shore uniform fringing reefs. In contrast to many previous studies, both the laboratory experiment and the numerical model account for the effects of large bottom roughness. The numerical model reproduced the observations of the wave transformation and runup over both smooth and rough reef profiles. The numerical model was then extended to quantify the influence of reef geometry and compared to simulations of plane beaches lacking a reef. For a fixed offshore forcing condition, the fore-reef slope controlled wave runup on reef-fronted beaches, whereas the beach slope controlled wave runup on plane beaches. As a result, the coastal protection utility of reefs is dependent on these slopes. For our examples, with a fore-reef slope of 1/5 and a 500 m prototype reef flat length, a beach slope of ∼1/30 marked the transition between the reef providing runup reduction for steeper beach slopes and enhancing wave runup for milder slopes. Roughness coverage, spacing, dimensions, and drag coefficient were investigated, with results indicating the greatest runup reductions were due to tall roughness elements on the reef flat.

Plain Language Summary Wave breaking and bottom friction are effective at reducing incident sea-swell waves before they can reach the shoreline of reef-fronted coastlines. However, globally, mass mortality of coral reef-building organisms is causing coral reefs to become structurally flatter, a process that may lower wave dissipation. Laboratory flume experiments and a multilayer phase-resolving wave-flow model that includes drag forces generated by roughness elements (representing coral reef forms) were used to investigate wave-driven water levels in the lee of fringing reefs and assess the influence of reef geometry and roughness characteristics. The numerical model was able to reproduce laboratory observations of waves and water levels over both smooth and rough reef profiles. Wave runup, the vertical extent of wave uprush on a beach, was sensitive to the presence and characteristics of roughness. Roughness coverage, spacing, and dimensions were investigated with results indicating the greatest runup reductions were due to tall roughness elements on the reef flat.

1. Introduction

Shallow fringing coral reefs have long been recognized as playing an important role in reducing wave energy reaching shorelines, and thus mitigating wave-driven coastal flooding (e.g., Munk & Sargent, 1948). Incident sea-swell (*SS*, <27 s periods) waves often break on shallow reefs and the large bottom roughness generated by the structural complexity of the reef results in high rates of *SS* wave dissipation (Harris et al., 2018; Monismith et al., 2015; Quataert et al., 2015). These processes contribute to a reduction in wave runup on reef-fronted beaches (Baldock et al., 2014; Quataert et al., 2015; Sheppard et al., 2005; Storlazzi et al., 2019). This has led to

21699291, 2022, 11, Downloaded from https://agupubs.onlinelibrary.wiley.com/doi/10.1029/2022JC018857 by Technical University Delft, Wiley Online Library on [07/12/2022]. See the Terms and Conditions (https://onlinelibrary.wiley.com/terms-and-conditions) on Wiley Online Library for rules of use; OA articles are governed by the applicable Creative Commons License

efforts to either restore coral reefs or build submerged structures to mimic reefs to protect vulnerable coastlines from wave-driven flooding (Ferrario et al., 2014; Reguero et al., 2018). However, infragravity waves (*IG*, >27 s periods) and wave setup generated during the *SS* wave breaking process also contribute to wave runup and can exceed the runup contribution from *SS* waves on both coasts with (Buckley et al., 2018a; Merrifield et al., 2014) and without reefs (Ruggiero et al., 2004; Stockdon et al., 2006). As both surf zone *IG* wave generation and wave setup are enhanced by *SS* wave dissipation, the intense *SS* wave breaking observed on many coral reefs can lead to large *IG* waves and wave setup (Becker et al., 2016; Buckley et al., 2018a; Pomeroy et al., 2012). Certain reef geometries can also trap and resonantly amplify specific *IG* frequencies leading to enhanced coastal flooding (Becker et al., 2016; Buckley et al., 2018a; Demirbilek et al., 2009; Gawehn et al., 2016; Merrifield et al., 2014; Pearson et al., 2017; Péquignet et al., 2009; Roeber & Bricker, 2015; Shimozono et al., 2015).

Reef flat resonance occurs at specific wave frequencies (natural modes) where the wavelength of standing waves reflected from the shoreline match the cross-shore reef geometry (Lugo-Fernández et al., 1998). At these frequencies, standing waves have an anti-node at the shoreline and a node at the reef crest. When this spatial pattern occurs, wave energy can be trapped between the reef crest and the shoreline, and each new wave propagating from offshore onto the reef flat adds energy to the trapped wave (i.e., resonant amplification) (Roeber & Bricker, 2015). The amount of resonant amplification, as measured by the increase in incoming wave height on the reef flat compared to the nonresonant case, is dependent on the reflection coefficients for incoming waves at the shoreline and outgoing waves at the reef crest, and frictional wave dissipation. It can be difficult to measure resonant amplification from laboratory or field observations, given that the nonresonant incoming wave height is generally unknown, leading to qualitative criteria for identifying resonance characteristics over reefs (Buckley et al., 2018a; Gawehn et al., 2016; Pomeroy et al., 2012).

Bottom roughness is a another key factor in the coastal protection utility of reef as it dissipates both *SS* and *IG* waves (Becker et al., 2016; Monismith et al., 2015) and lowers shoreline wave setup for reefs with onshore directed near-bed currents (Rijnsdorp et al., 2021). Coral degradation and the loss of coral cover are expected to reduce the capacity for reefs to accrete vertically, which will also result in a decline in structural complexity; the reef surface will become deeper and structurally flatter (Alvarez-Filip et al., 2009; Perry & Alvarez-Filip, 2019; Sheppard et al., 2005; Storlazzi et al., 2018). This raises questions about the ability of coral reefs to maintain their coastal protection utility in the face of rising sea levels and declining heath. It is therefore crucial to understand the mechanisms controlling wave-driven flooding on reefs and develop validated tools to predict wave runup.

When validated, the use of numerical hydrodynamic models can be applied to: (a) elucidate many coastal processes that are difficult to quantify in field and laboratory experiments, (b) predict how these processes may change in the future, and (c) determine their relative impact on wave runup, which is of particular importance to quantify the risk of coastal flooding for different scenarios. Several classes of numerical models have been applied to simulate wave transformations and flows over coral reefs. Spectral (phase-averaged) wave models coupled to flow models have been shown to describe the evolution of the statistical properties of *SS* waves, as well as the effect of bulk wave forces on mean flows (currents) (Filipot & Cheung, 2012; Lindhart et al., 2021; Lowe et al., 2009a; Torres-Garcia et al., 2018). However, these models do not resolve wave runup, and they also neglect the processes that describe *IG* waves, which are generated when wave groups of *SS* waves break on reefs (Pomeroy et al., 2012; Symonds et al., 1982). These *IG* waves have been shown to be important and, in some cases, dominant near the shoreline (Becker et al., 2016; Buckley et al., 2018a; Péquignet et al., 2009; Pomeroy et al., 2012; Roeber & Bricker, 2015). To efficiently simulate *IG* waves in nearshore applications, surfbeat models, which couple *SS* wave models with flow models on the time scale of wave groups, were developed (Quataert et al., 2015; Roelvink et al., 2009; van Dongeren et al., 2013). Whilst the wave runup from wave setup and *IG* swash is computed by these surfbeat models, *SS* swash motions are neglected or parameterized, which can result in substantial inaccuracies in the prediction of runup (Buckley et al., 2018a; Lashley et al., 2018; Pearson et al., 2017; Quataert et al., 2020). Finally, phase-resolving wave-flow models that treat waves and flow simultaneously have also been applied (Buckley et al., 2014; Lowe et al., 2019; Ma et al., 2014; Rijnsdorp et al., 2021; Roeber & Cheung, 2012; Yao et al., 2012, 2020a, 2021; Zijlema, 2012). This class of model varies widely in terms of complexity and computational cost, ranging from single-layer models to fully three-dimensional (3D) computational fluid dynamics (CFD) models. Nonhydrostatic wave-flow models are popular for modeling wave runup, due to the balance between computational efficiency and the ability to capture the relevant physical processes (e.g., Franklin & Torres-Freyermuth, 2022; Quataert et al., 2020).

21699291, 2022, 11, Downloaded from https://agupubs.onlinelibrary.wiley.com/doi/10.1029/2022JC018857 by Technical University Delft, Wiley Online Library on [07/12/2022]. See the Terms and Conditions (https://onlinelibrary.wiley.com/terms-and-conditions) on Wiley Online Library for rules of use; OA articles are governed by the applicable Creative Commons License

21699291, 2022, 11, Downloaded from https://agupubs.onlinelibrary.wiley.com/doi/10.1029/2022JC018857 by Technical University Delft, Wiley Online Library on [07/12/2022]. See the Terms and Conditions (https://onlinelibrary.wiley.com/terms-and-conditions) on Wiley Online Library for rules of use; OA articles are governed by the applicable Creative Commons License

A number of laboratory, field, and numerical model studies have been undertaken to quantify the effectiveness of reefs at reducing wave runup (Baldock et al., 2014; Ferrario et al., 2014; Pearson et al., 2017; Quataert et al., 2015). However, a major limitation of many of these studies has been the lack of a detailed accounting of the effects of large bottom roughness on wave-driven hydrodynamics. In laboratory studies, most experiments have focused on recreating only the large-scale morphology of reefs using smooth beds (and hence associated modeling studies have neglected roughness), which is not representative of many natural coral reefs (Buckley et al., 2014; Demirbilek et al., 2009; Lashley et al., 2018; Pearson et al., 2017; Yao et al., 2012; Zijlema, 2012). While in most field studies, the large natural roughness is often difficult to geometrically quantify, which when combined with sparse hydrodynamic observations, has led to the roughness being quantified based on gradients in energy flux (Lentz et al., 2016; Lowe, Falter, et al., 2005; Monismith et al., 2015; Pomeroy et al., 2012). This approach is replicated in numerical models, where various empirical coefficients to parameterize bulk bottom drag coefficients are used as model tuning parameters (Lowe et al., 2009a; van Dongeren et al., 2013), which may differ between models and even one-dimensional (1D) and two-dimensional (2D) implementations of the same model (van Dongeren et al., 2013).

Recent advances in several multilayer phase-resolving wave-flow models create the opportunity to incorporate more robust descriptions of how wave-driven flows interact with large bottom roughness. For example, the multilayer nonhydrostatic wave-flow model SWASH (Simulating WAves till Shore; Zijlema et al., 2011), which is used in this present study, has recently been extended to include a canopy flow model that enables simulations of the effect of large roughness elements on wave and mean flow dynamics (Suzuki et al., 2019). Such canopy flow models are often used for aquatic vegetation and attempt to simulate the spatially averaged flow within canopies by accounting for forces on canopy elements (Jadhav et al., 2013; Lowe et al., 2007; Nepf & Vivoni, 2000). Importantly, these canopy flow models can explain the frequency dependence of drag dissipation across reefs (e.g., Lowe et al., 2005), due to how higher-frequency wave motions are able to drive larger oscillatory flows in canopies, resulting in larger drag forces and hence greater rates of wave dissipation (Lowe et al., 2007). This is particularly important for understanding the impact of differences in reef roughness geometry.

In this study, we investigate how different reef and shoreline geometries, roughness properties, and wave conditions interact on fringing reefs and influence wave runup. In Section 2, we first describe the data set of Buckley et al. (2016), which was a set of laboratory experiments that investigated the effect of large roughness on wave and wave setup dynamics. The canopy flow model within SWASH is next introduced along with the methods we used to encapsulate canopy processes as well as to determine the different contributions to wave runup. In Section 3, we start by comparing the numerical model results to the laboratory experiment data set. We then present results from the validated model setup for a range of different cases. We first consider the impact of the fore-reef slope and beach slope and then evaluate how the presence of a reef effects wave runup. This analysis includes quantification of resonant amplification of low-frequency waves by comparing incoming reef flat wave heights between simulations with (resonant) and without (nonresonant) a reflective beach. Finally, we assess the spatial and geometric impact of reef roughness. In Section 4, we conclude with a discussion on the coastal protection opportunity afforded by a reef in comparison to an ocean-exposed beach, consider how future changes in reef roughness are likely to affect coastal flooding along reef-fringed shorelines, and consider to what extent a relatively smooth reef can be considered to offer a coastal protection benefit.

2. Methods

2.1. Laboratory Setup

Buckley et al. (2016) undertook laboratory experiments in a 55-m long wave flume to investigate the effect of large roughness on wave transformation, setup dynamics, and wave runup on a scaled physical model of a fringing reef (Figure 1; Buckley et al., 2018b). The reef profile was based on a typical fringing reef (see Quataert et al., 2015), with a 1:5 fore-reef slope, a 14-m horizontal reef flat, and a 1:12 sloped beach (Figure 1). For the 1:36 geometric scaling factor used, the reef flat of the model was equivalent to a 500-m reef at field (prototype) scale. TMA spectrums (Bouws et al., 1985) of irregular waves were generated with a piston-type wavemaker that featured second-order wave generation and active reflection compensation (van Dongeren et al., 2002).

A range of conditions (from typical to extreme) were simulated by varying the still water depths, wave heights, and wave periods (Table 1). Deep water wave parameters were estimated from observations at the wave gauge

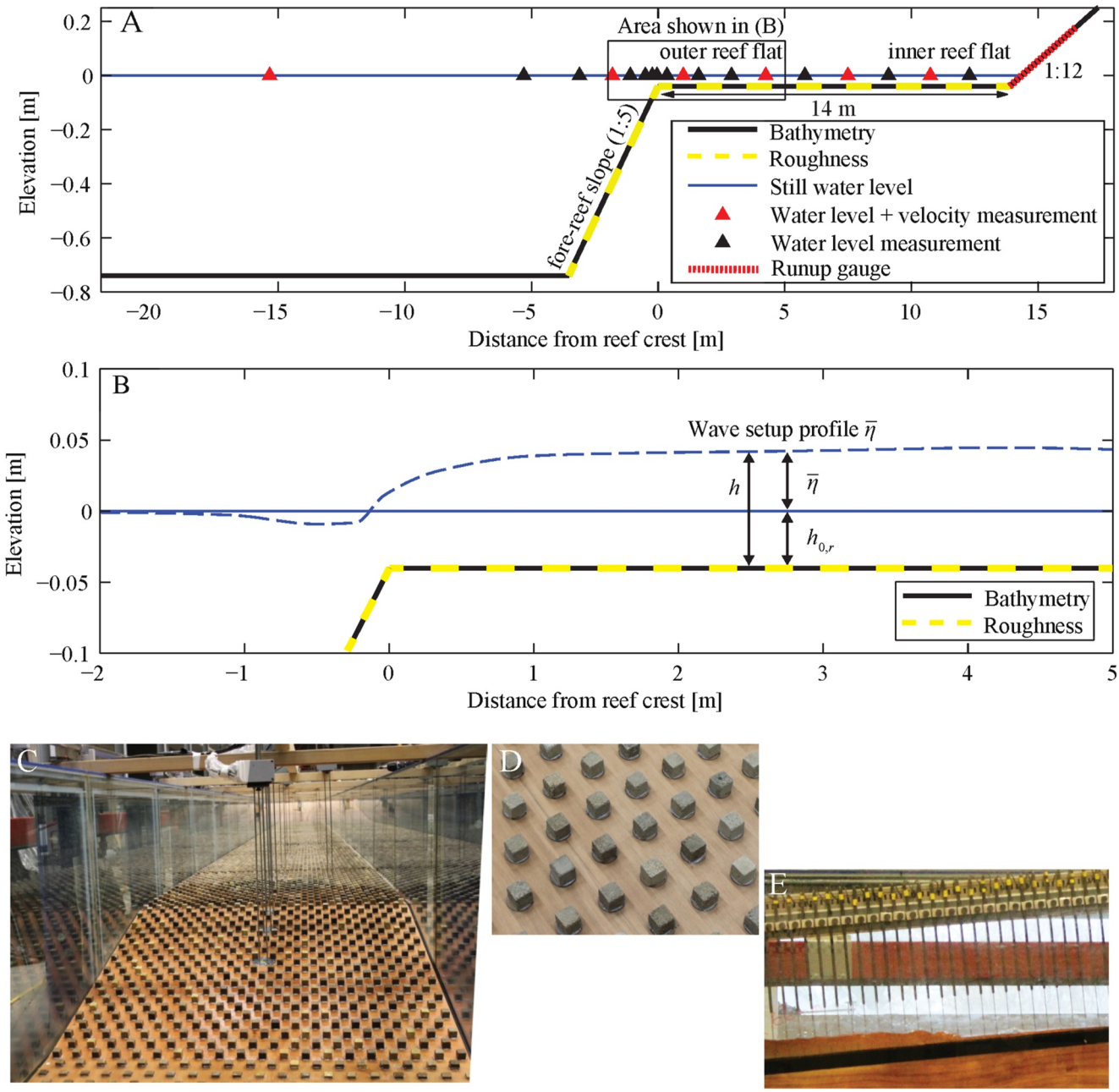

Figure 1. (a) Schematic of the fringing reef showing the fore-reef slope (1:5), reef flat length (14 m; ~500 m field scale), beach slope (1:12), and instrument locations. Sections of the bathymetry (reef slope and reef flat) highlighted in dashed yellow were affixed with roughness elements as shown in (c) and (d). (b) An example of the wave setup profile $\overline{\eta}$ in the vicinity of the reef crest, defining the still water depth over the reef $h_{0,r}$ and the total water depth h. (c) View of the dry flume with (d) roughness elements. The photo was taken looking shoreward from offshore of the reef slope. (e) Runup gauge consisting of resistance wires at a 25 mm spacing along the slope (1.7 mm vertical resolution).

nearest the wavemaker ($x = -15.34$ m) using linear wave theory. Two sets of 16 runs were conducted during the experiment. The first set of runs used a smooth plywood bottom to minimize the role of bottom roughness (Buckley et al., 2015). In the second set of runs, a staggered array of 1.8 cm concrete cubes (equivalent to 65 cm at field scale) were affixed to the plywood on the fore-reef slope and reef flat (Figure 1b). These concrete blocks were a proxy for the bottom roughness characteristics often observed on coral reefs (Buckley et al., 2016). Both sets of experiments used a smooth nonporous beach.

21699291, 2022, 11, Downloaded from https://agupubs.onlinelibrary.wiley.com/doi/10.1029/2022JC018857 by Technical University Delft, Wiley Online Library on [07/12/2022]. See the Terms and Conditions (https://onlinelibrary.wiley.com/terms-and-conditions) on Wiley Online Library for rules of use; OA articles are governed by the applicable Creative Commons License

Table 1
Simulated Wave and Water Level Conditions Including the Deep Water Sea-Swell rms Wave Height ($H_{rms,SS,0}$), the Peak Wave Period (T_p), the Still Water Depth on the Reef Flat ($h_{0,r}$), the Peak Deep Water Wave Steepness ($H_{rms,SS,0}/L_0$), and the Deep Water Surf Similarity Parameter ($\xi_{0,r}$) Calculated Using the Fore-Reef Slope

	Lab scale			Field scale				
	$H_{rms,SS,0}$	T_p	$h_{0,r}$	$H_{rms,SS,0}$	T_p	$h_{0,r}$	$H_{rms,SS,0}/L_0$	$\xi_{0,r}$
Run	[m]	[s]	[m]	[m]	[s]	[m]	[–]	[–]
1	0.03	2.26	0.04	1.1	13.6	1.4	0.004	3.3
2	0.06	2.26	0.04	2.2	13.6	1.4	0.007	2.4
3	0.09	2.26	0.04	3.2	13.6	1.4	0.011	1.9
4	0.12	2.26	0.04	4.3	13.6	1.4	0.015	1.7
5	0.14	2.26	0.04	5.0	13.6	1.4	0.018	1.5
6	0.17	2.26	0.04	6.1	13.6	1.4	0.021	1.4
7	0.06	1.31	0.04	2.2	7.9	1.4	0.021	1.4
8	0.06	3.20	0.04	2.2	19.2	1.4	0.004	3.4
9	0.06	2.26	0.00	2.2	13.6	0.0	0.009	2.2
10	0.06	2.26	0.02	2.2	13.6	0.7	0.009	2.2
11	0.06	2.26	0.06	2.2	13.6	2.2	0.008	2.3
12	0.06	2.26	0.09	2.2	13.6	3.2	0.008	2.3
13	0.12	2.26	0.00	4.3	13.6	0.0	0.015	1.7
14	0.12	2.26	0.02	4.3	13.6	0.7	0.015	1.7
15	0.12	2.26	0.06	4.3	13.6	2.2	0.015	1.7
16	0.12	2.26	0.09	4.3	13.6	3.2	0.015	1.6

Note. Deep water wave parameters were estimated from observations at the wave gauge nearest the wavemaker ($x = -15.34$ m) using linear wave theory. Parameter values are given for both the laboratory scale (1:36 geometric scaling and 1:6 scaling of time) and the equivalent field scale.

Along the flume, water levels (18 locations with resistance-type gauges) and horizontal velocities (6 locations with electromagnetic current meters) were measured synchronously at 40 Hz. These time series were then down-sampled to 20 Hz for comparison with SWASH outputs. The experimental runs were 41 min (2,460 s) in duration with only the last 33 min (1,980 s) used for analysis. Wave runup was measured using an array of resistance-type gauges along the beach slope with 0.025 m spacing for the first 1 m of the gauge and 0.05 m spacing for the remaining 1.2 m (Raichlen & Hammack, 1975; van Gent, 2001).

2.2. Numerical Model

The multilayer nonhydrostatic wave-flow model SWASH is a numerical implementation of the Reynolds-averaged Navier-Stokes equations for an incompressible fluid with a constant density (Zijlema et al., 2011). This model describes the free-surface as singled-valued and is thus less computationally expensive than fully 3D (i.e., CFD) models. In a 2D vertical plane, the governing equations in Cartesian, cross-shore (x) and vertical (z) coordinates and time (t) are (Suzuki et al., 2019; Zijlema et al., 2011):

$$\frac{\partial u}{\partial t} + \frac{\partial uu}{\partial x} + \frac{\partial wu}{\partial z} = -\frac{1}{\rho}\frac{\partial (P_h + P_{nh})}{\partial x} + \frac{\partial \tau_{xx}}{\partial x} + \frac{\partial \tau_{xz}}{\partial z} - \frac{1}{\rho}F_x, \quad (1)$$

$$\frac{\partial w}{\partial t} + \frac{\partial uw}{\partial x} + \frac{\partial ww}{\partial z} = -\frac{1}{\rho}\frac{\partial P_{nh}}{\partial z} + \frac{\partial \tau_{zz}}{\partial z} + \frac{\partial \tau_{zx}}{\partial x}, \text{ and} \quad (2)$$

$$\frac{\partial u}{\partial x} + \frac{\partial w}{\partial z} = 0, \quad (3)$$

where $u(x,z,t)$ and $w(x,z,t)$ are the horizontal and vertical velocities, respectively; ρ is water density; P_h and P_{nh} are the hydrostatic and nonhydrostatic pressures, respectively, and τ_{xx}, τ_{xz}, τ_{zz}, and τ_{zx} are the Reynolds (turbulent) stresses. The last term in Equation 1 represents the canopy drag force per unit cross-shore area (F_x) that is exerted on the flow, which is parametrized using the Morison equation and includes both form drag and inertial force term (Suzuki et al., 2019):

$$F_x = 0.5\rho C_D \lambda_f |u|u + \rho(1 + C_m)\, h_c \lambda_p \frac{\partial u}{\partial t} \quad (4)$$

where C_D is a drag coefficient and C_m is the added-mass coefficient associated with an individual roughness element.

In Equation 4, the geometric properties of the roughness elements are defined by the horizontal dimensions both normal (l_w) and parallel (l_l) to the wave-flow field, the vertical dimension (h_c), and the density of roughness elements N_c (i.e., the number of roughness elements per unit plan area). From these variables, the remaining two nondimensional parameters in Equation 4 are defined as:

$$\lambda_f \equiv l_w h_c N_c, \text{ and}$$
$$\lambda_p \equiv l_w l_l N_c, \quad (5)$$

where λ_f is the frontal area of roughness elements per unit plan area and λ_p is the plan area of the roughness elements per unit plan area. For the array of cubes used in the Buckley et al. (2016) experiment, $N_c = 400$ m^{-2}, $l_w = l_l = h_c = 1.8$ cm, and $\lambda_f = \lambda_p = 0.13$ (Figure 1). Furthermore, Buckley et al. (2016) estimated $C_D = 1.5$ and $C_m = 1$ for the concrete cubes used in the experiment. When these values are compared to those reported for branched reef corals by Lowe, Koseff, and Monismith (2005) ($\lambda_f = 0.42$–6.31 and $\lambda_p = 0.02$–0.38), we note that λ_f in the laboratory experiments is smaller, but that λ_p is comparable. From the dimensions and spacing of the

21699291, 2022, 11, Downloaded from https://agupubs.onlinelibrary.wiley.com/doi/10.1029/2022JC018857 by Technical University Delft, Wiley Online Library on [07/12/2022]. See the Terms and Conditions (https://onlinelibrary.wiley.com/terms-and-conditions) on Wiley Online Library for rules of use; OA articles are governed by the applicable Creative Commons License

21699291, 2022, 11, Downloaded from https://agupubs.onlinelibrary.wiley.com/doi/10.1029/2022JC018857 by Technical University Delft, Wiley Online Library on [07/12/2022]. See the Terms and Conditions (https://onlinelibrary.wiley.com/terms-and-conditions) on Wiley Online Library for rules of use; OA articles are governed by the applicable Creative Commons License

roughness elements and a representative wave forcing, Buckley et al. (2016) calculated a wave friction factor (f_w) of 0.16 using the canopy flow equations of Lowe et al. (2007). This is within the typical range of f_w observed in many field studies of coral reefs; for example, $f_w = 0.15$ (Nelson, 1996), $f_w = 0.22$ (Falter et al., 2004), and $f_w = 0.24$ (Lowe, Falter, et al., 2005).

The numerical model was configured with a uniform horizontal grid size of 0.05 m and an initial time step of 0.005 s. Subsequent time steps were adjusted to stay within the specified range of Courant numbers from 0.1 to 0.6. Twenty evenly spaced vertical sigma layers were used; the high vertical resolution allows for the development of steep wave faces and the initiation of wave breaking without the need of the hydrostatic front approximation to initiate breaking (Smit et al., 2013). A logarithmic wall law near the bed is assumed with a Nikuradse roughness height of 4×10^{-4} used for the plywood bed. For simulations with canopy roughness elements, the canopy model (Equation 4) is also implemented. The vertical mixing was modelled with a $k - \varepsilon$ turbulence model (Launder & Spalding, 1974) in combination with a constant vertical eddy viscosity (1×10^{-5}).

For each of the laboratory runs, the numerical simulations were forced with the Fourier components of the incoming wave time series calculated from co-located wave and velocity measurements nearest the wavemaker. For parameter space simulations looking at reef geometry and roughness, the forcing conditions from Run 2 were simulated. Run 2 had an intermediate wave height, period, and water level (Table 1). The data produced by the numerical models were defined to be consistent with the laboratory experiments: simulations were 41 min (2,460 s) with the last 33 min (1,980 s) used for analysis, the water level and velocity time-series data were exported at 20 Hz, and wave runup time series were extracted as the most landward point with a water depth greater than 0.004 m to correlate with the resolution of the wave runup gauge used in the experiment. To assess the model performance, we quantified the relative bias (*RB*) and Murphy's skill score (Murphy, 1988; *MS*) statistics:

$$RB = \frac{\frac{1}{N}\sum_{n=1}^{N}(Q_p - Q_o)}{\frac{1}{N}\sum_{n=1}^{N} Q_o}, \tag{6}$$

$$MS = 1 - \frac{\sum_{n=1}^{N}(Q_p - Q_o)^2}{\sum_{n=1}^{N}\left(Q_o - \overline{Q}_o\right)^2} \tag{7}$$

where N is the total number of observations and Q is the considered quantity with subscripts p and o denoting predicted and observed values, respectively. Lower values of *RB* indicate better performance and $MS < 0.5$, $0.5 < MS < 0.75$ and $MS > 0.75$ representing poor, moderate, and high prediction scores, respectively (Hansen et al., 2015).

2.3. Data Analysis

The data from both the laboratory and numerical models were analyzed in a similar way. Wave and swash spectra were computed from water level measurements using Welch's modified periodogram method with a Hanning window and a segment length of 2^{14} samples (820 s). The spectra were divided into sea-swell (*SS*; $f \geq f_p/2$) and infragravity (*IG*; $f < f_p/2$) frequency ranges, where f_p is the peak forcing frequency of each run. To examine the natural frequencies of the reef flat, the *IG* spectra were further divided into a high infragravity (IG_H; $f_p/2 > f \geq 0.060$ Hz) and low infragravity (IG_L; $f < 0.060$ Hz) band. At field scales, the division between *SS* and *IG* is equivalent to 0.037 Hz (27 s period) for the default wave forcing (Table 1), and the division between IG_H and IG_L corresponds to 0.010 Hz (100 s period). The separation frequency of IG_H and IG_L was chosen to isolate the first two natural frequencies (that are also most likely to resonantly amplify) of the reef flat within the IG_L frequency band (Buckley et al., 2018a). Following Buckley et al. (2015), incoming and outgoing waves were separated at six locations with synchronous water level and velocity measurements using a frequency domain algorithm, which assumes the linear wave theory transfer function between water level and velocity. This method is similar to Guza et al. (1984), but because it operates in the frequency domain, using linear wave theory for the wave celerity it can be used without the need for a shallow water assumption.

To quantify the wave runup at the shoreline, the individual runup maxima (peaks) were identified by assessing if each maxima was significantly larger than the points around it based on a specified minimum prominence of 0.003 m, chosen to represent the sensitivity of the laboratory wave runup gauge. The 2% wave runup ($R_{2\%}$), which

21699291, 2022, 11, Downloaded from https://agupubs.onlinelibrary.wiley.com/doi/10.1029/2022JC018857 by Technical University Delft, Wiley Online Library on [07/12/2022]. See the Terms and Conditions (https://onlinelibrary.wiley.com/terms-and-conditions) on Wiley Online Library for rules of use; OA articles are governed by the applicable Creative Commons License

is the value exceeded by the largest 2% of runup maxima in the runup distribution, was then determined from the cumulative distribution function (Stockdon et al., 2006).

2.4. Cases Considered

The Buckley et al. (2016) laboratory experiments were limited to a single reef geometry and roughness configuration. Here, we reproduce these experiments and then extend the model to investigate the role that these parameters more generally play over a much wider range of possible scenarios. Model roughness covers a range of values that could be representative of different coral restoration scenarios or natural variability in the distribution, size, shape, and abundance (density) of corals. At individual sites, coral reef degradation may reduce coral cover and coral reef recovery, or restoration may increase coral cover. Here we investigate spatial variability in coverage, roughness element spacing (N_c), volume ($l_w l_l h_c$), height (h_c), and assigned drag coefficient (C_D).

The model is also used to investigate a range of different reef geometries and still water depths. Typically for shallow reefs, the important slope to consider is the fore-reef slope where wave breaking is concentrated. However, beach slope on reef-fronted coasts is also important for both wave runup and reef flat wave dynamics due to wave reflection from the shoreline. We used the SWASH model to investigate the impact of both the fore-reef slope and the beach slope. Three fore-reef slopes were investigated within the range of natural reef slopes from relatively mild (1:20) to steep (1:1) (Falter et al., 2013; Quataert et al., 2015). Responses to beach slope were investigated with several slopes from mild (1:400) to steep (1:5) (Guza et al., 1984). To quantify the impact of a beach slope with and without a reef, we conducted identical simulations to Run 2 with varying beach slopes with and without the reef structure. The impact of the fore-reef slope and beach slope was quantified using the Iribarren number, $\xi_0 = \beta/\sqrt{H_{rms,0}/L_0}$ where β is slope of either the fore-reef slope or the beach slope, which gives an indication of if and how waves will break on a slope. It can also provide an indication of the extent of wave reflection and the theoretical maximum possible swash amplitude (Carrier & Greenspan, 1958; Raubenheimer & Guza, 1996). Two distinct Iribarren numbers, $\xi_{0,r}$ and $\xi_{0,b}$ are used to quantify the impact of fore-reef slope and the beach slope, respectively.

3. Results

3.1. Wave Dynamics and Model Performance for a Representative Run

The inspection of results for one representative case (Run 2; Table 1) reveals the rapid wave transformation and wave setup generation that occurs over the reef profile (Figures 2 and 3). SWASH was generally able to reproduce the wave observations (including the incoming and outgoing directionally separated wave components) and frequency distribution (*SS*, IG_H, and IG_L). This includes the strong shoaling and rapid dissipation of *SS* waves at the reef crest (Figures 2a and 3a) and the corresponding wave set-down and setup (Figures 2d and 3d). We note that the wave gauge at $x = -0.23$ m, produced higher wave heights and more wave set-down than predicted by SWASH. Similar discrepancies were also noted for this particular wave gauge by Lashley et al. (2018) and Lowe et al. (2022).

The inclusion of roughness for this same representative case increased wave dissipation, which was captured by the numerical model (Figure 3). The most notable deviation between the laboratory and numerical model results occurs for the incoming component of $H_{rms,IGL}$ for both smooth and rough runs, where there is an underprediction in incoming $H_{rms,IGL}$ seaward of the reef crest and an overprediction in incoming $H_{rms,IGL}$ landward of the reef crest. This suggests a slight mismatch in the boundary conditions and either an overprediction of IG_L surf zone generation or insufficient dissipation. Decomposition of the hydrodynamic data into its frequency composition reveals that SWASH generally reproduced the evolution of different frequency components across the reef experiment and model domain (Figure 4). The spectra show a clear *SS* dominance offshore of the reef crest (Figures 4a and 4b) and the strong *IG* dominance across the reef flat for both the total and incoming components (Figure 4). A standing wave pattern is observed in the *IG* frequencies in both the laboratory and numerical data (Figure 4).

The total (incoming + outgoing) IG_H and IG_L wave heights (Figures 2–4) and spectra (Figure 4) exhibit standing wave patterns resulting from the superposition of incoming and outgoing waves across the reef. Standing wave nodes appear as local minima and anti-nodes as maxima (Buckley et al., 2018a). When the total hydrodynamic signals are decomposed into their incoming and outgoing components, the generation, dissipation, and

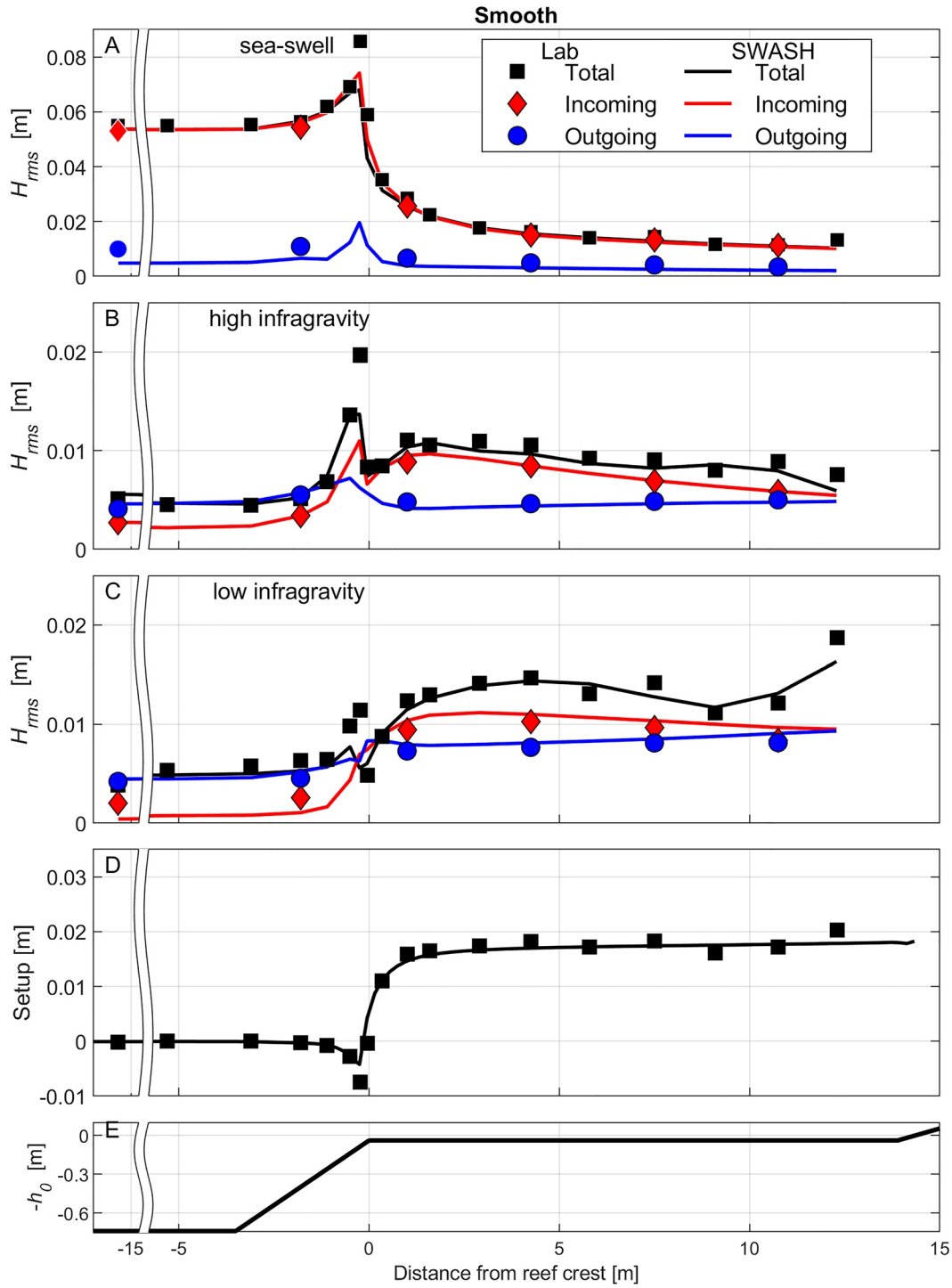

Figure 2. Comparison of predicted and observed (a) sea-swell, (b) high infragravity, and (c) low infragravity *rms* wave heights, and (d) wave setup across (e) the fringing reef profile for Run 2 without bed roughness (smooth). Incoming/outgoing separation required co-located water level and velocity measurements, and hence, could only be computed at a subset of wave gauge locations for the experimental data.

reflection of the IG_H and IG_L are revealed (Figures 2–4). The incoming *SS* waves are strongly dissipated across the reef. The outgoing *SS* wave component was small but showed some reflection (and de-shoaling) from the reef crest and some minimal reflection from the beach (Figures 2a and 3a), consistent with *SS* wave breaking and

21699291, 2022, 11, Downloaded from https://agupubs.onlinelibrary.wiley.com/doi/10.1029/2022JC018857 by Technical University Delft, Wiley Online Library on [07/12/2022]. See the Terms and Conditions (https://onlinelibrary.wiley.com/terms-and-conditions) on Wiley Online Library for rules of use; OA articles are governed by the applicable Creative Commons License

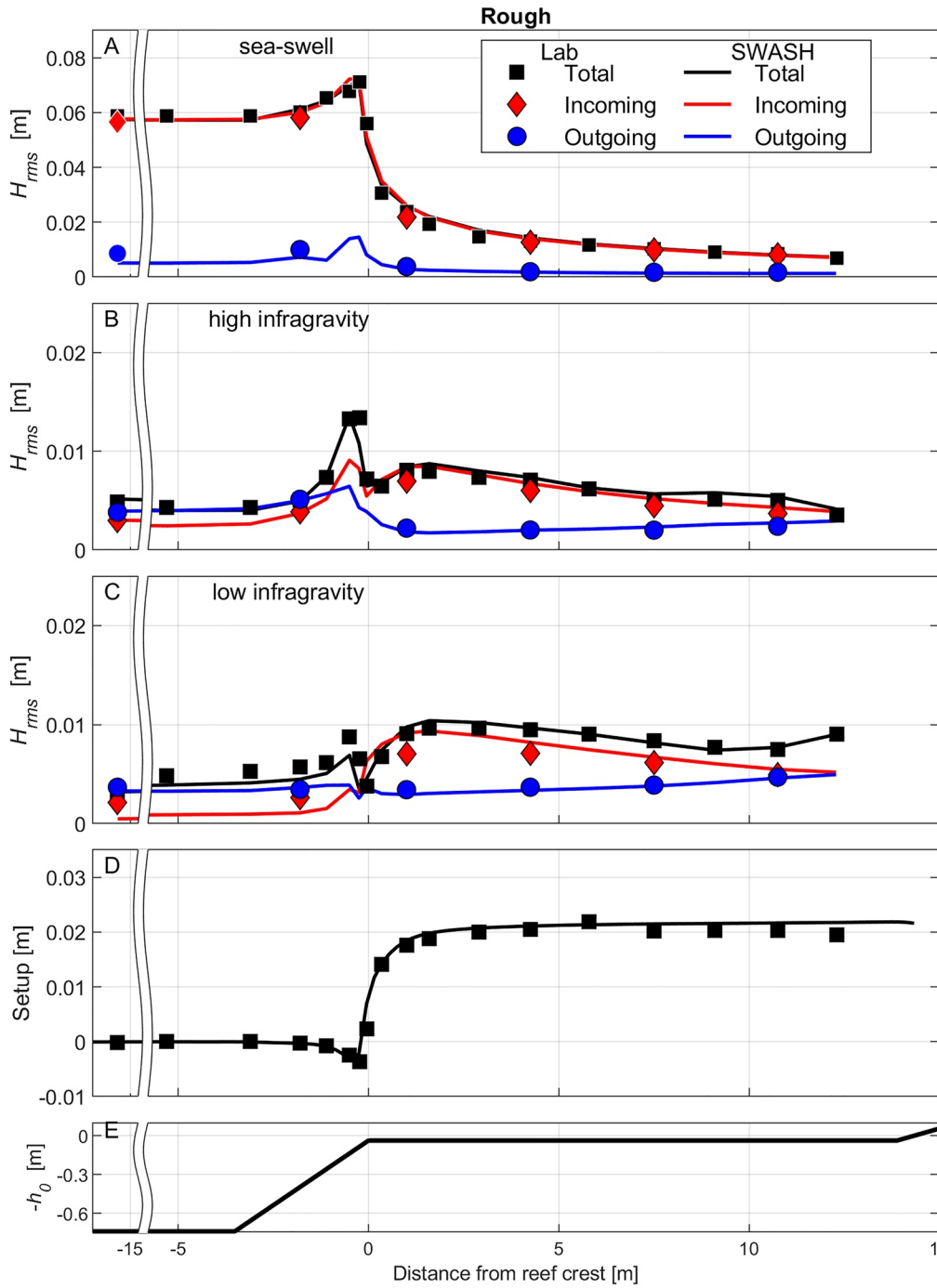

Figure 3. Same as Figure 2, but with the rough bed. Comparison of predicted and observed (a) sea-swell, (b) high infragravity, and (c) low infragravity *rms* wave heights, and (d) wave setup across (e) the fringing reef profile for Run 2 with bed roughness. Incoming/outgoing separation required co-located water level and velocity measurements, and hence, could only be computed at a subset of wave gauge locations for the experimental data.

(with roughness present) frictional dissipation over the reef. In contrast, the incoming IG_H and IG_L wave heights increase through the surf zone with incoming IG_H reaching a maximum at the *SS* breakpoint and incoming IG_L reaching a maximum on the outer reef flat. The IG_H and IG_L waves reflect at the shoreline, with reflection coefficients near 1 at the most landward directional wave gauge (x = 10.75 m). When roughness is included, there is greater dissipation of the incoming and outgoing *SS*, IG_H, and IG_L waves over the fore-reef and reef flat

21699291, 2022, 11, Downloaded from https://agupubs.onlinelibrary.wiley.com/doi/10.1029/2022JC018857 by Technical University Delft, Wiley Online Library on [07/12/2022]. See the Terms and Conditions (https://onlinelibrary.wiley.com/terms-and-conditions) on Wiley Online Library for rules of use; OA articles are governed by the applicable Creative Commons License

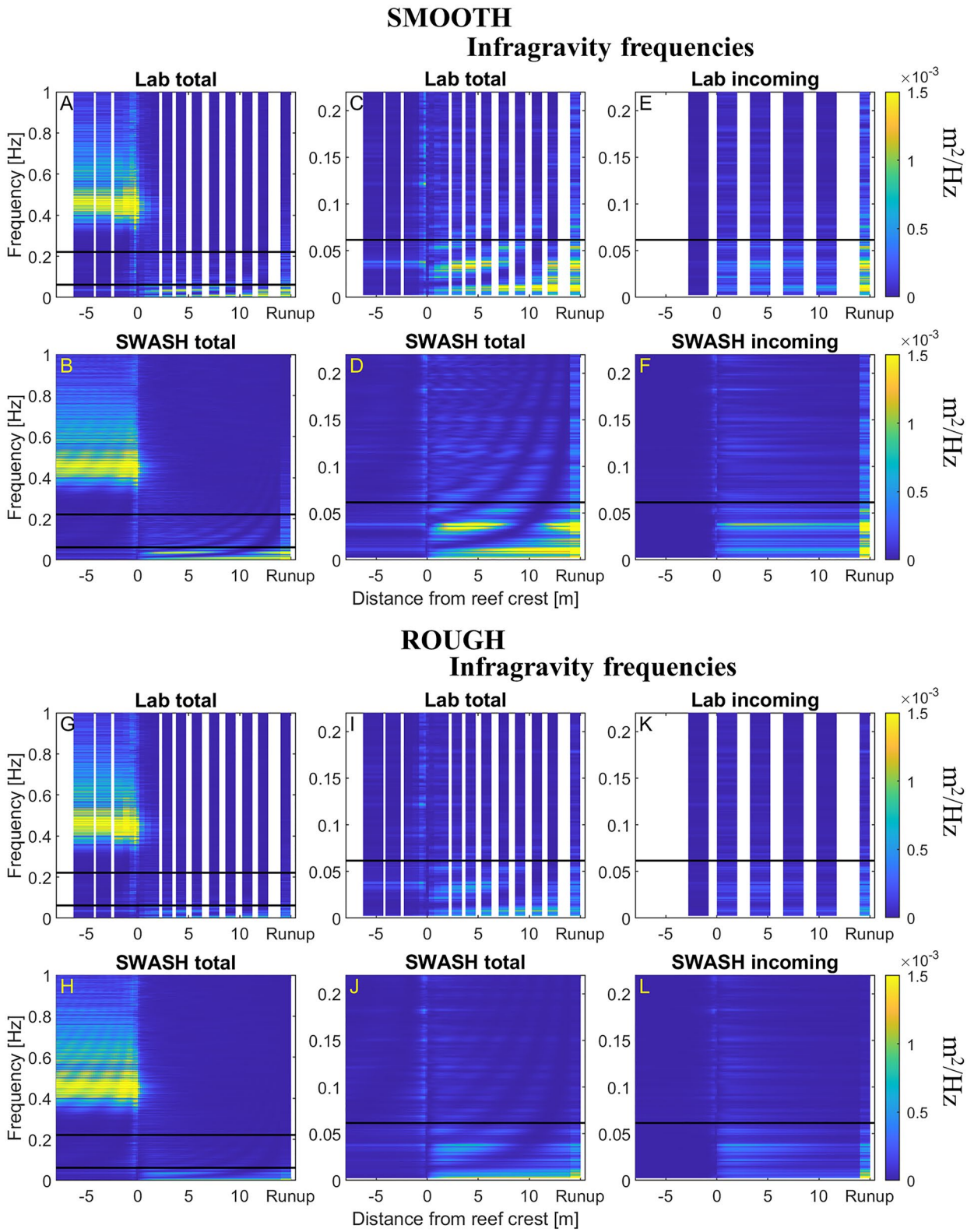

Figure 4. Power spectral density of the measured and predicted waves and only the incoming wave component for smooth and rough Run 2. Horizontal black lines give the cutoff frequencies between sea-swell, high infragravity, and low infragravity. Note that columns two and three are zoomed in to only show infragravity frequencies. White columns in (a), (c), (e), (g), (i), and (k) are due to the spacing of wave gauges in the laboratory study.

21699291, 2022, 11, Downloaded from https://agupubs.onlinelibrary.wiley.com/doi/10.1029/2022JC018857 by Technical University Delft, Wiley Online Library on [07/12/2022]. See the Terms and Conditions (https://onlinelibrary.wiley.com/terms-and-conditions) on Wiley Online Library for rules of use; OA articles are governed by the applicable Creative Commons License

Table 2
The Relative Biases (RB) and Murphy Skill Scores (MS) in rms Wave Height and Wave Setup Across All Runs (Table 1) and Wave Gauges (Figure 1)

	Smooth		Rough	
	RB	*MS*	*RB*	*MS*
H_{rms}	−0.050	0.97	−0.0088	0.98
$H_{rms,SS}$	−0.056	0.98	−0.020	0.98
$H_{rms,IGH}$	−0.053	0.93	0.0062	0.92
$H_{rms,IGL}$	−0.054	0.88	0.066	0.78
$\overline{\eta}$	0.0011	0.98	0.033	0.98
$R_{2\%}$	0.052	0.91	0.17	0.78
$R_{2\%} - \overline{R}$	−0.0085	0.82	0.20	0.71
$\overline{R}$	0.13	0.85	0.15	0.74

Note. *RB* and *MS* are also given for 2% exceedance wave runup ($R_{2\%}$), the swash contribution to runup ($R_{2\%} - \overline{R}$) and wave setup at the shoreline ($\overline{R}$).

(Figure 3). For this rough reef case, the incoming wave heights on the inner reef flat ($x = 10.75$ m) were reduced (on average) by 29%, 40%, and 44% for *SS*, IG_H, and IG_L, respectively, compared to the corresponding smooth reef case.

3.2. Model Performance Across All Runs

The numerical model SWASH reproduced the bulk wave parameters observed in the laboratory experiments (Table 2 and Figure 5). When averaged over all wave gauge sites, Murphy skill scores (*MS*) indicate high prediction scores ($MS \geq 0.78$) for total, *SS*, IG_H, and IG_L *rms* wave heights across all runs for both the smooth and rough simulations. At the directional wave gauge closest to the beach ($x = 10.75$ m), where the numerical results are particularly important for coastal flooding, there was generally good agreement between the observed and modeled *SS*, IG_H, and IG_L *rms* wave heights (Figures 5a–5c). However, modeled IG_L *rms* wave heights deviated from the smooth observations at higher values, with a wider range of values observed in the laboratory results compared to the simulations (Figure 5c). Wave setup had high predictive scores ($MS = 0.98$) for both smooth and rough simulations (Table 1 and Figure 5d).

The 2% wave runup was predicted with high predictive scores for both smooth ($MS = 0.91$) and rough runs ($MS = 0.78$) (Table 2 and Figure 5e). Despite excellent agreement with wave setup at the wave gauges (Table 2 and Figure 5d), a slight overprediction of mean runup ($\overline{R}$) was observed (Figure 5g). The swash component of runup ($R_{2\%} - \overline{R}$) was also slightly overpredicted for runs with roughness (Table 2 and Figure 5f). Overall, the modeled $R_{2\%} - \overline{R}$ and $\overline{R}$ received high predictive scores for the smooth runs ($MS \geq 0.82$) and moderate predictive scores for the runs with roughness ($MS \geq 0.71$).

3.3. Numerical Simulations With Varying Fore-Reef Slope (β_r)

Here, we use the validated numerical model to explore reef geometries not included in the Buckley et al. (2016) experiment. These simulations use the default forcing conditions from Run 2 and vary either fore-reef slope or beach slope. The numerical model results for varying fore-reef slopes, which considered the three natural reef slopes from relatively mild (1:20) to steep (1:1) (Falter et al., 2013; Quataert et al., 2015), indicate that wave heights on the reef flat across all frequencies (*SS*, IG_H, and IG_L) and wave setup increase with fore-reef slope (Figure 6). Thus, the fore-reef slope plays a crucial role in controlling wave setup and the height of the incident waves that propagate across the reef and ultimately result in wave runup. The difference between wave setup on the smooth and rough reefs was less on the lower 1/20 reef slope profile than it was on the steeper 1/5 and 1/1 reef slope profiles. This is due to the balance between the reduced mean wave forces with roughness present and the increased time-averaged bottom drag forces (Buckley et al., 2016).

3.4. Numerical Simulations With Varying Beach Slope (β_b)

Beach slope had an interesting effect on the reef flat waves (Figure 7). At the lowest beach slope tested ($\beta_b = 1/400$), nearly all the wave energy that was not dissipated on the reef profile was dissipated on the beach slope, likely due to breaking (van Dongeren et al., 2007). This dissipation reduced the amplitude of reflected waves compared with the steeper beach slope ($\beta_b = 1/12$) used in the laboratory experiment across all frequencies, including IG_L where evidence of resonant amplification was found in the laboratory observations for this same experiment by Buckley et al. (2018a). With $\beta_b = 1/400$, the reduced outgoing wave energy on the reef flat lowered the total IG_H and IG_L wave heights and eliminated the standing wave pattern in reef flat IG_H and IG_L wave heights (Figures 7b and 7c). There was little observed change in incoming *rms* wave height on the reef flat for the Run 2 forcing conditions and across all runs (Figures 7c and 8). However, wave runup was typically greater for the steeper beach slope case (Figure 9).

21699291, 2022, 11, Downloaded from https://agupubs.onlinelibrary.wiley.com/doi/10.1029/2022JC018857 by Technical University Delft, Wiley Online Library on [07/12/2022]. See the Terms and Conditions (https://onlinelibrary.wiley.com/terms-and-conditions) on Wiley Online Library for rules of use; OA articles are governed by the applicable Creative Commons License

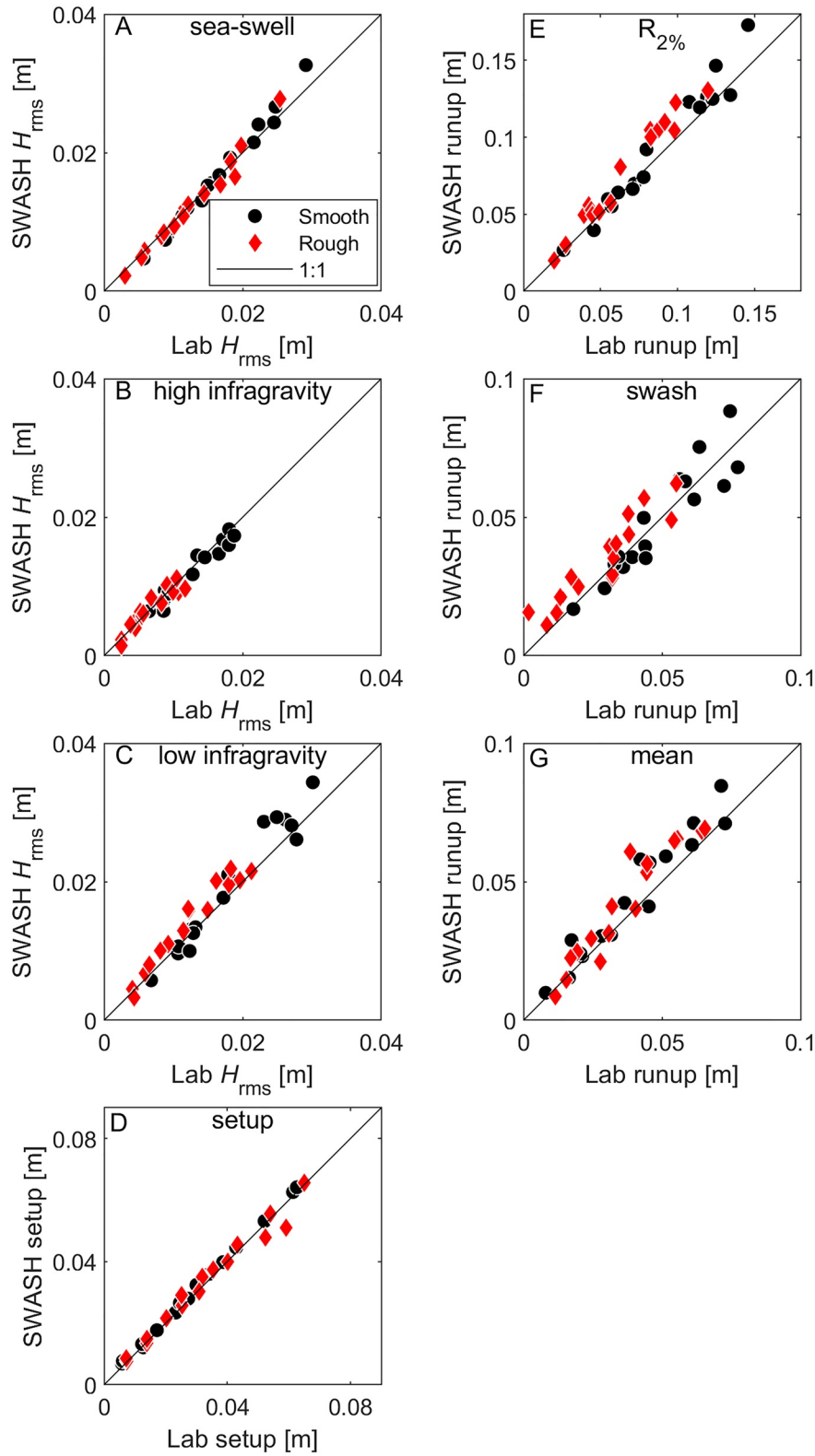

Figure 5. Comparison between observed and predicted (a) sea-swell, (b) high infragravity, and (c) low infragravity *rms* wave heights, and (d) wave setup at the directional wave gauge nearest the shoreline (x = 10.75 m). Comparison between observed and predicted (e) 2% exceedance runup and its components (f) 2% exceedance swash and (g) the mean components (wave setup at the shoreline). All smooth (black circles) and rough (red diamonds) runs (Table 1) are shown.

21699291, 2022, 11, Downloaded from https://agupubs.onlinelibrary.wiley.com/doi/10.1029/2022JC018857 by Technical University Delft, Wiley Online Library on [07/12/2022]. See the Terms and Conditions (https://onlinelibrary.wiley.com/terms-and-conditions) on Wiley Online Library for rules of use; OA articles are governed by the applicable Creative Commons License

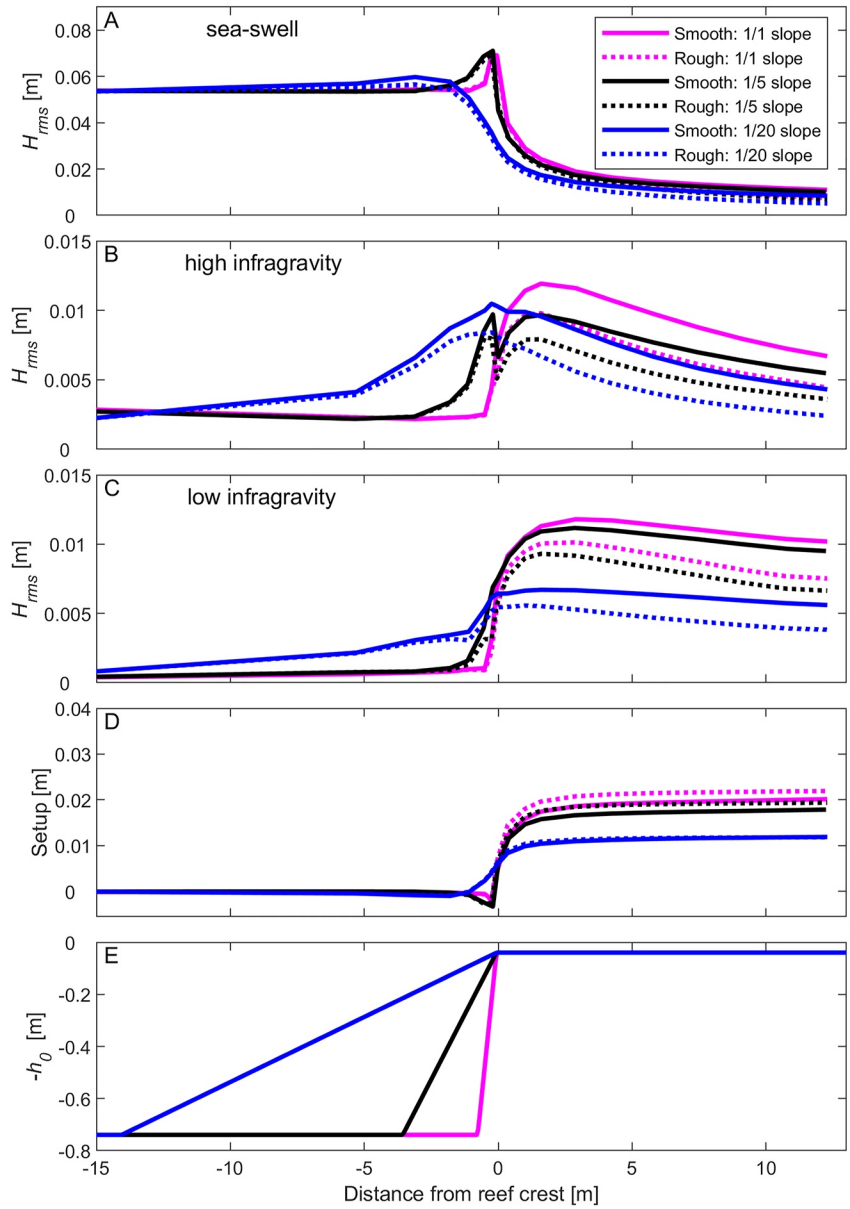

Figure 6. Incoming (a) sea-swell, (b) high infragravity, and (c) low infragravity *rms* wave heights and (d) wave setup predicted by SWASH for (e) fringing reef profiles with varying reef slopes and with (dashed curves) and without (solid curves) roughness. The forcing conditions, reef flat length, and beach slope from Run 2 were used.

3.5. Wave Runup Simulations on Beaches With and Without Reefs

Simulations of a beach with the same forcing conditions as the default Run 2 with and without a reef exhibited different runup extents depending on the beach slope, which was varied (Figure 9). For the particular reef geometry and forcing conditions tested here, a reef-fronted beach with a mild slope (β_b < ~1/30; Figure 9a) was observed to have larger wave runup than a plane beach of the same slope. However, as the beach slope was increased, the wave runup on the plane beaches increased rapidly and quickly exceeded the runup observed for an equivalent beach fronted by a reef. Particularly for the rough reef-fronted beaches tested here, beach slope had little effect on either total wave runup or the swash and wave runup components (Figure 8). In contrast, wave runup and swash peaked at $\xi_{0,b} \approx 6$ ($\beta_b \approx 1/2$), and wave setup peaked at $\xi_{0,b} \approx 3$ ($\beta_b \approx 1/4$) for the open coast beach cases. At $\xi_{0,b} \approx 6$, the reef reduced wave runup by 67% and 73% for smooth and rough simulations, respectively.

21699291, 2022, 11, Downloaded from https://agupubs.onlinelibrary.wiley.com/doi/10.1029/2022JC018857 by Technical University Delft, Wiley Online Library on [07/12/2022]. See the Terms and Conditions (https://onlinelibrary.wiley.com/terms-and-conditions) on Wiley Online Library for rules of use; OA articles are governed by the applicable Creative Commons License

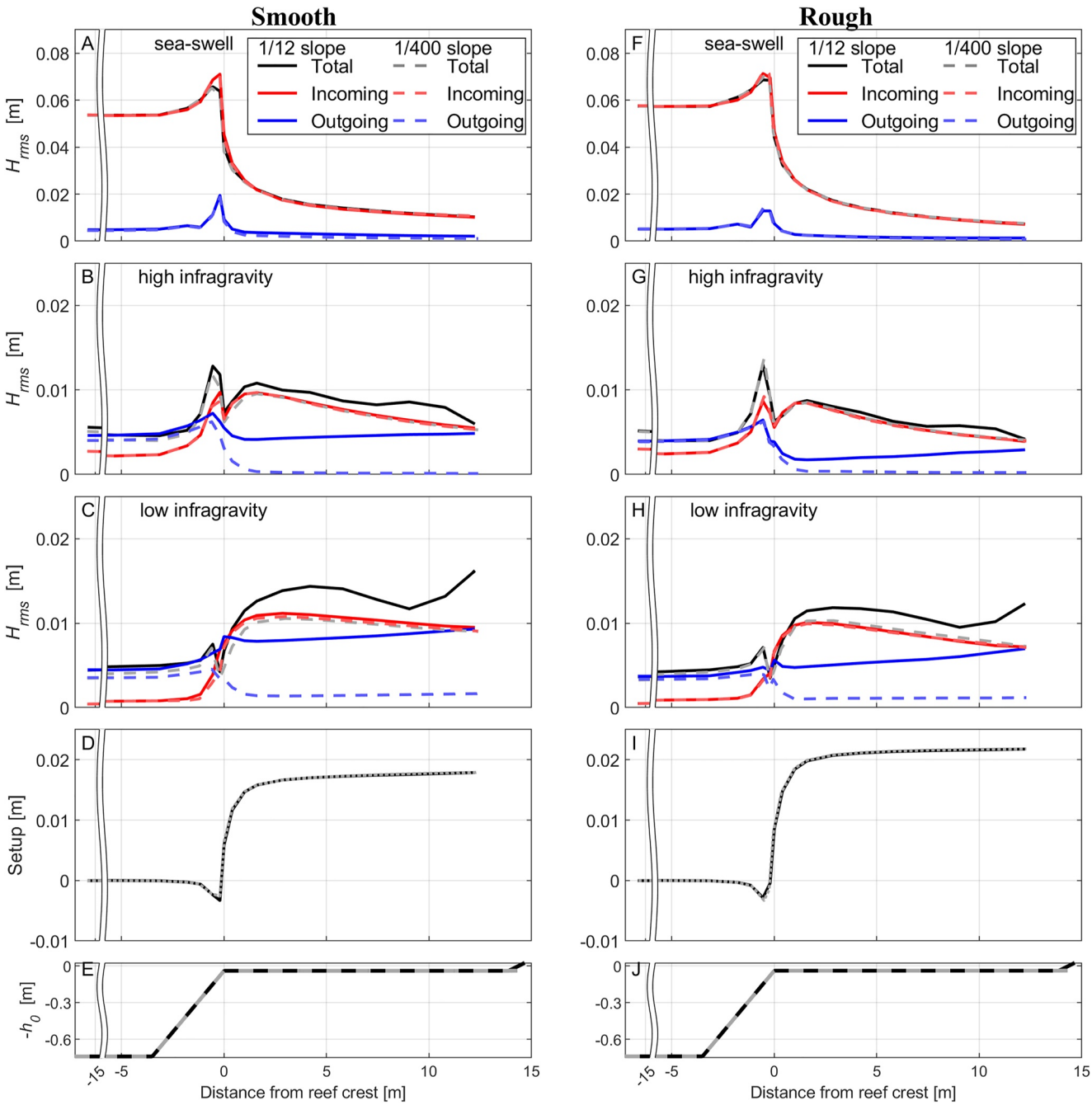

Figure 7. Comparison of SWASH results for smooth (column 1) and rough (column 2) Run 2 with the 1/12 beach slope used in the laboratory experiment (solid curves) and with a lower 1/400 beach slope to minimize reflection at the shoreline (dashed curves). Results are shown for (a, f) sea-swell, (b, g) high infragravity, and (c, h) low infragravity *rms* wave heights, and (d, i) wave setup across (e, j) the fringing reef profiles. Due to the enhanced shoreline reflection with the 1/12 beach slope, total *rms* wave height in the infragravity frequencies have a standing wave pattern, whereas with the dissipative 1/400 beach, outgoing wave heights are low and total *rms* wave height is mainly controlled by the incoming component.

3.6. Wave Runup Simulations With Varying Still Water Depth ($h_{0,r}$)

Unlike plane beaches, varying still water depth on reef profiles can have a large effect on wave runup and its components (Figure 10). The swash component of runup initially increased for the reef profiles when the still water depth was increased until values stabilized at approximately the equivalent plane beach value when $h_{0,r}$ was approximately four times $H_{rms,0}$ (Figure 10b). The swash component of runup was smaller for the rough runs relative

21699291, 2022, 11, Downloaded from https://agupubs.onlinelibrary.wiley.com/doi/10.1029/2022JC018857 by Technical University Delft, Wiley Online Library on [07/12/2022]. See the Terms and Conditions (https://onlinelibrary.wiley.com/terms-and-conditions) on Wiley Online Library for rules of use; OA articles are governed by the applicable Creative Commons License

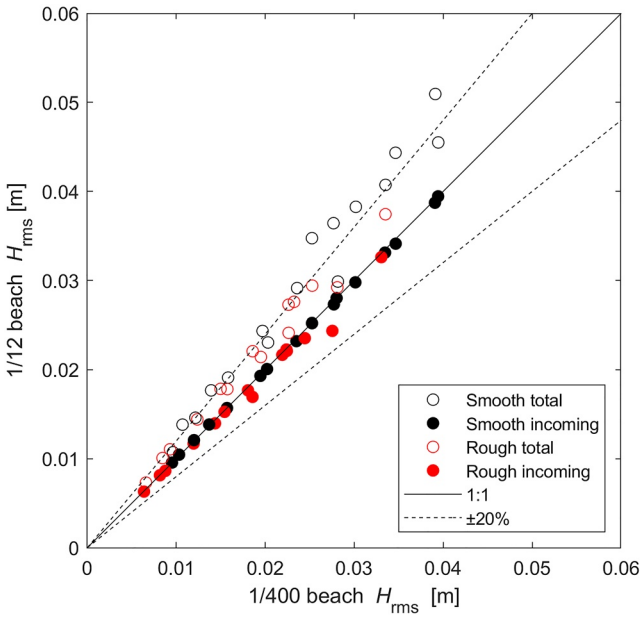

Figure 8. Comparison total (open circle) and incoming (solid circles) *rms* wave height near the shoreline ($x = 10.75$ m) for smooth (black) and rough (red) SWASH simulations with a 1/400 beach slope (x-axis) and a 1/12 beach slope (y-axis) for all forcing conditions (Table 1). Due to the enhanced shoreline reflection with the 1/12 beach slope total *rms* wave heights typically fall above the 1:1 line (solid black line). Whereas the incoming *rms* wave height is relatively unaffected by the change in beach slope with points typically near the 1:1 line.

to the smooth runs for all cases, with the greatest reduction at low still water depths and a fairly uniform reduction after $h_{0,r}$ was approximately two times $H_{rms,0}$ (equivalent to $h_{0,r}$ three times the roughness height). Wave setup on the reef flat decreased rapidly to zero with increased still water depth (Figure 10c). However, wave setup at the shoreline showed a parabolic response to still water depth with the largest values at low and high still water depths and a minimum at $h_{0,r}$ equal to $H_{rms,0}$. Reef flat wave setup was similar for smooth and rough runs. Shoreline wave setup was also similar for rough and smooth runs at low still water depths, but shoreline wave setup was reduced for the rough runs compared to the smooth runs for $h_{0,r}$ greater than $H_{rms,0}$.

3.7. Numerical Simulations With Varying Roughness

The laboratory experiments used either uniformly smooth or uniformly rough reef profiles; however, a natural reef exhibits spatial roughness variability. Here we compare the spatially uniform cases to a reef with a smooth reef slope and a rough reef flat and to a reef with a rough reef slope and a smooth reef flat. As expected, the uniformly smooth reef generated the least wave dissipation and the uniformly rough reef generated the most wave dissipation (Figure 11). The case with the smooth slope and rough reef flat showed larger wave heights on the fore-reef than the rough slope and smooth reef flat case. However, these trends were reversed over the reef flat. Wave setup was the greatest for the smooth slope and rough reef flat case (Figure 11d). With the addition of roughness, Buckley et al. (2016) identified two mechanisms affecting wave setup over fringing reefs with roughness: (a) the reduction of surf zone radiation stress gradients from frictional dissipation and (b) time-averaged bottom drag forces from the interaction of waves and undertow with roughness enhancing wave setup. The smooth slope and rough reef flat case are ideal for wave setup generation, as surf zone radiation stress gradients are not impacted by frictional dissipation, but wave setup is enhanced by time-averaged bottom drag forces on the reef flat. Wave runup ($R_{2\%}$) was 0.060 m for the fully smooth reef case and 0.050 m for the fully rough case (17% decrease from smooth case). The $R_{2\%}$ was 0.053 m for the smooth reef slope and rough reef flat (11% decrease from smooth), and 0.057 m for the rough reef slope and smooth reef flat (6% decrease from smooth).

Modifying the spacing (N_c), volume ($l_w l_l h_c$), height (h_c), and assigned drag coefficient (C_D) had varying impacts on specific hydrodynamic components (Figure 12). Increasing the number of roughness elements from smooth (0) to 100 elements per m^{-2} ($\lambda_f = \lambda_p = 0.032$) resulted in a large increase in wave dissipation, primarily on the reef flat. The influence was similar for all wave frequencies (Figures 12a–12c). A further increase in the number of roughness elements (up to $\lambda_f = \lambda_p = 0.26$) resulted in little increase in wave dissipation. This was likely due to the close spacing of roughness elements diverting flow over the canopy rather than through the canopy where drag forces are generated that dissipate wave energy (Lowe et al., 2007). While the increased number of elements increased the wave setup, this increase was small (<10% for the range considered; Figure 12d).

Increasing the volume of the cube-shaped roughness elements (up to $\lambda_f = \lambda_p = 0.51$) decreased the fore-reef and reef flat wave heights significantly (Figures 12e–12g). However, as the volume of roughness elements increased there was an increase in wave setup (Figure 12h). This would diminish some of the coastal protection benefits from the high volume roughness elements. Increasing the height h_c of the roughness elements had the greatest impact on the wave dissipation and setup (Figures 12i–12l); taller roughness elements resulted in larger dissipation but had more variable impacts on wave setup. This increased dissipation was associated with the increased total frontal area of roughness elements and the reduction of the relative submergence of the roughness $h_c/(h_0 + \bar{\eta})$. While wave setup initially increased with the height of the roughness, when the roughness became emergent, a substantial reduction in setup was observed (Figure 12l). Finally, varying the assigned C_D had little effect on wave setup but did affect wave dissipation (Figures 12m–12p). For example, when the C_D was twice as large as in the laboratory experiments (3 vs. 1.5), wave setup near the shoreline decreased by 3% and the incoming *rms* wave heights decreased by 17%. We note that the shorter the wave period (i.e., *SS* vs. IG_L), the greater the wave dissipation.

21699291, 2022, 11, Downloaded from https://agupubs.onlinelibrary.wiley.com/doi/10.1029/2022JC018857 by Technical University Delft, Wiley Online Library on [07/12/2022]. See the Terms and Conditions (https://onlinelibrary.wiley.com/terms-and-conditions) on Wiley Online Library for rules of use; OA articles are governed by the applicable Creative Commons License

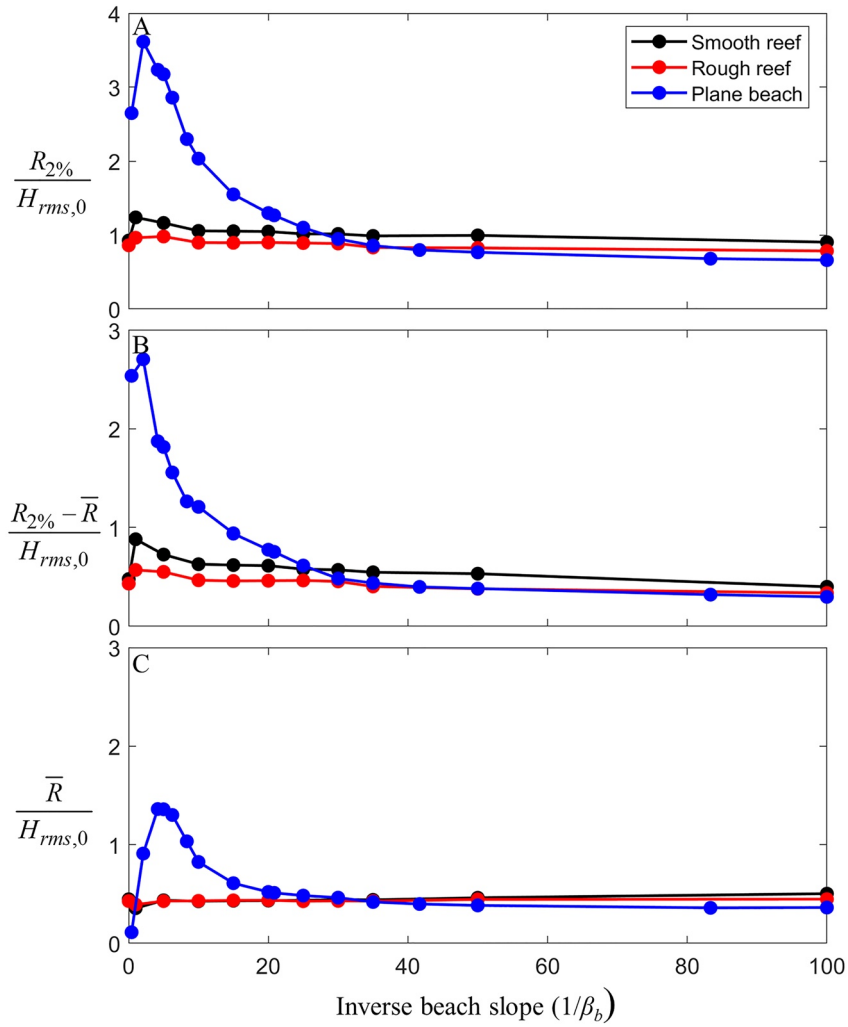

Figure 9. Trends in (a) 2% exceedance wave runup, (b) 2% exceedance swash, and (c) wave setup at the shoreline with each normalized by deep water *rms* wave height versus the inverse beach slope ($1/\beta_b$). Results are shown for smooth (black) and rough (red) reef profiles with a 1/5 fore-reef slope, a 500 m prototype reef flat length, and varying beach slopes. These results are compared to plane beach simulations without a reef (blue). Run 2 forcing conditions where used (Table 1) with a fixed deep water wave height and wavelength and only the beach slope varied. Note that $1/\beta_b$ was used for plotting purposes to better display steep beach slopes.

4. Discussion

This study has demonstrated that a shallow fringing reef can significantly reduce *SS* waves reaching a shoreline while at the same time generating substantial *IG* wave energy and wave setup that may offset some of the protective benefits of reefs in reducing overall wave runup. Due to the competing role of these factors, this raises the question: to what degree does the presence of a reef fronting a beach reduce wave-driven coastal flooding (extreme runup) when compared to an open-coast beach, and what role does reef roughness have?

4.1. Influence of Reef Geometry

On open coast beaches, wave breaker type and wave runup normalized by deep water wave height are known to vary with deep water wave steepness and beach slope, which is quantified using the Iribarren number (Battjes, 1974b). According to Battjes (1974a), for plane beaches, the wave breaker type varies according to $\xi_{0,b} < 0.5$ spilling, $0.5 < \xi_{0,b} > 3.3$, and $\xi_{0,b} < 3.3$ surging or collapsing. The wave runup normalized by deep water wave height

21699291, 2022, 11, Downloaded from https://agupubs.onlinelibrary.wiley.com/doi/10.1029/2022JC018857 by Technical University Delft, Wiley Online Library on [07/12/2022]. See the Terms and Conditions (https://onlinelibrary.wiley.com/terms-and-conditions) on Wiley Online Library for rules of use; OA articles are governed by the applicable Creative Commons License

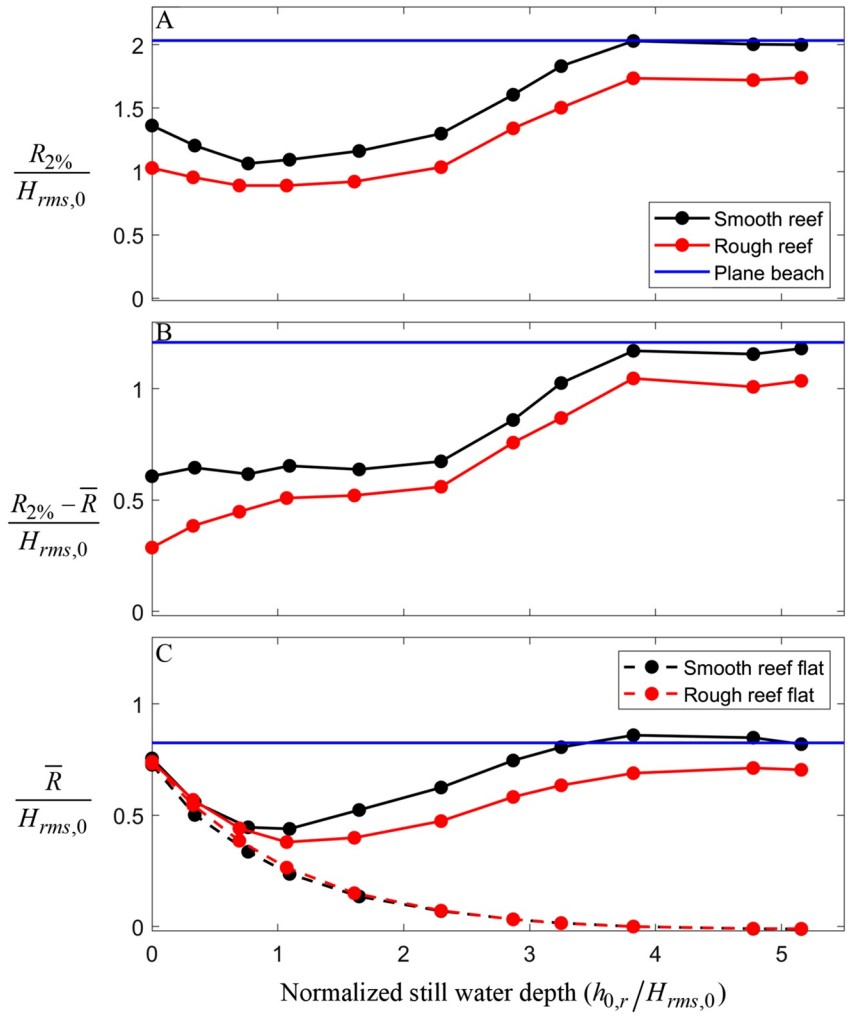

Figure 10. Trends in (a) 2% exceedance wave runup, (b) 2% exceedance swash, and (c) wave setup on the reef flat (dashed curves) and shoreline (solid curves) versus still water depth on the reef flat. Each quantity is normalized by deep water *rms* wave height. Results are shown for smooth (black) and rough (red) reef profiles and compared with a plane beach case with the same 1/12 beach slope (horizontal blue line). Run 2 forcing conditions where used (Table 1).

tends to increase with $\xi_{0,b}$ as wave type transitions from spilling to plunging and then peaks at the transition from plunging to surging (Hedges & Mase, 2004; Stockdon et al., 2006). This was observed in our SWASH simulations conducted using plane beaches of various slopes (Figure 9). At low $\xi_{0,b}$, conditions are dissipative; waves spill and most of the relatively low wave runup is generated by wave setup and *IG* swash (Figure 9) (Ruggiero et al., 2004). In the plunging range, wave runup is generated by both wave setup and *SS* and *IG* swash (Figure 9).

Compared to plane open coast beaches, reefs have more complex geometries and a greater range of bottom roughness. There are also fewer numerical and observational studies of wave runup on coral reef-lined coasts to help understand the parameters controlling and the physical drivers of wave runup. However, there have been several recent studies of wave runup on coral reef-lined coasts. In a numerical study of 1D coral reef geometries using single-layer nonhydrostatic XBeach, Pearson et al. (2017) found water depth over the reef flat, incident wave conditions, and the width of the reef flat had the most influence on wave runup, with runup being less sensitive to beach slope and bed friction. However, with the single-layer model, the time-averaged bottom drag forces generated by a combination of undertow and nonlinear waves, which Buckley et al. (2016) found was important for wave setup generation, would not have been captured. We also expect the canopy flow model used in this study to more closely match the effects of bottom roughness than the bed shear stress friction model used by Pearson et al. (2017). Using a multilayer SWASH model, Franklin and Torres-Freyermuth (2022) confirmed

21699291, 2022, 11, Downloaded from https://agupubs.onlinelibrary.wiley.com/doi/10.1029/2022JC018857 by Technical University Delft, Wiley Online Library on [07/12/2022]. See the Terms and Conditions (https://onlinelibrary.wiley.com/terms-and-conditions) on Wiley Online Library for rules of use; OA articles are governed by the applicable Creative Commons License

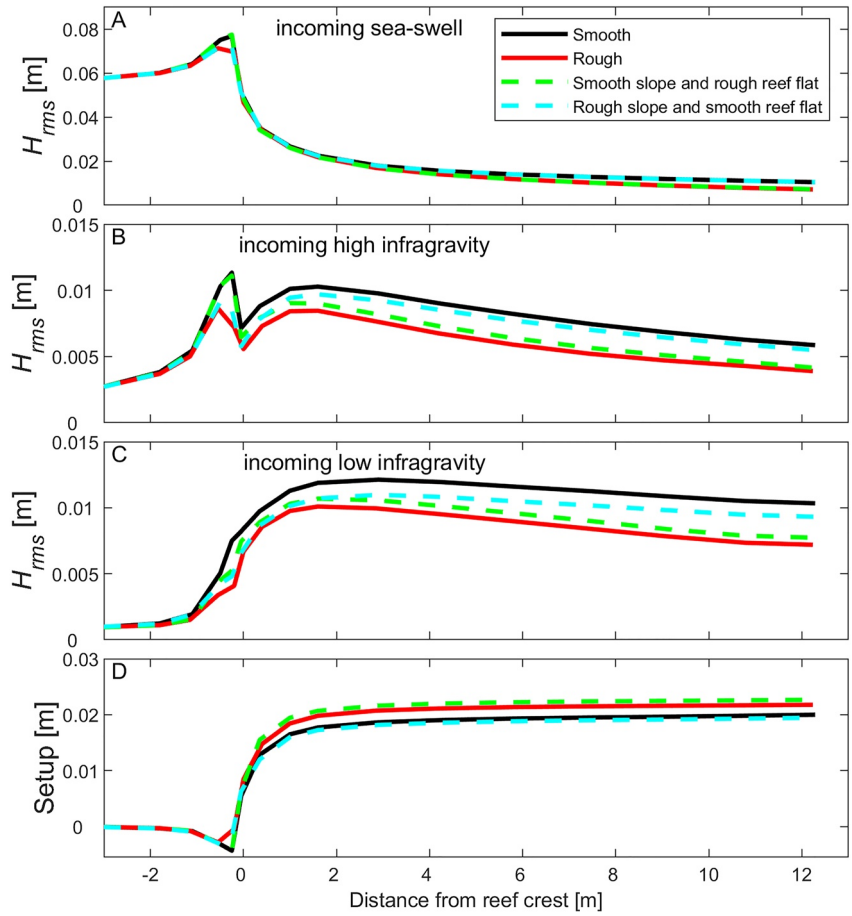

Figure 11. Incoming (a) sea-swell, (b) high infragravity, and (c) low infragravity root mean square wave heights H_{rms} and (d) wave setup for SWASH simulations with a smooth reef slope and reef flat (solid black curve), a rough reef slope and reef flat (solid red curve), a smooth reef slope and a rough reef flat (dashed magenta curve), and a rough reef slope and a smooth reef flat (dashed blue curve). The forcing conditions, fore-reef slope, reef flat length, and beach slope from Run 2 were used.

some of the results of Pearson et al. (2017), finding that wave height was the most important variable in predicting wave runup followed wave period, fore-reef slope, and reef flat depth. Reef flat length and reef crest height were found to be of lesser importance. However, Franklin and Torres-Freyermuth (2022) did not investigate the role of bottom roughness. We therefore seek to build on the analysis of Pearson et al. (2017) and Franklin and Torres-Freyermuth (2022) using a multilayer SWASH model with a canopy flow model to better understand the role of coral reef bottom roughness.

Our results show that the coastal protection utility provided by reefs varies with factors that include fore-reef slope, beach slope, and roughness characteristics and distribution. Natural reef slopes vary from relatively mild sloping to near vertical (Falter et al., 2013; Quataert et al., 2015). Our results show that the fore-reef slope affects the height of waves across all frequencies (*SS*, IG_H, and IG_L). Indeed, wave heights and wave setup both increase when the slope of the fore-reef increases (Figure 6). Based on the fore-reef slopes of 1/1, 1/5, and 1/20, $\xi_{0,r} = 12.1$ (nonbreaking), 2.4 (plunging breaking), and 0.6 (spilling breaking), respectively, with open coast breaking types given in parenthesis (Battjes, 1974b). In contrast to a uniform slope where waves with $\xi_{0,b} = 12.1$ would be expected to reflect without breaking, the *SS* wave reflection coefficient offshore of the reef was only 0.3, indicating that the majority of the rapid *SS* wave dissipation near the reef crest was due to *SS* waves breaking on the shallow reef crest. Consistent with this finding, wave setup on the reef flat increased with increased fore-reef slope (Figure 6d). The steeper surf zone bathymetry on the fore-reef generates larger radiation stress gradients from *SS* wave breaking in shallower water resulting in more wave setup (Bowen et al., 1968). Wave rollers formed in the *SS* breaking process may further enhance wave setup by transferring momentum into even shallower water

21699291, 2022, 11, Downloaded from https://agupubs.onlinelibrary.wiley.com/doi/10.1029/2022JC018857 by Technical University Delft, Wiley Online Library on [07/12/2022]. See the Terms and Conditions (https://onlinelibrary.wiley.com/terms-and-conditions) on Wiley Online Library for rules of use; OA articles are governed by the applicable Creative Commons License

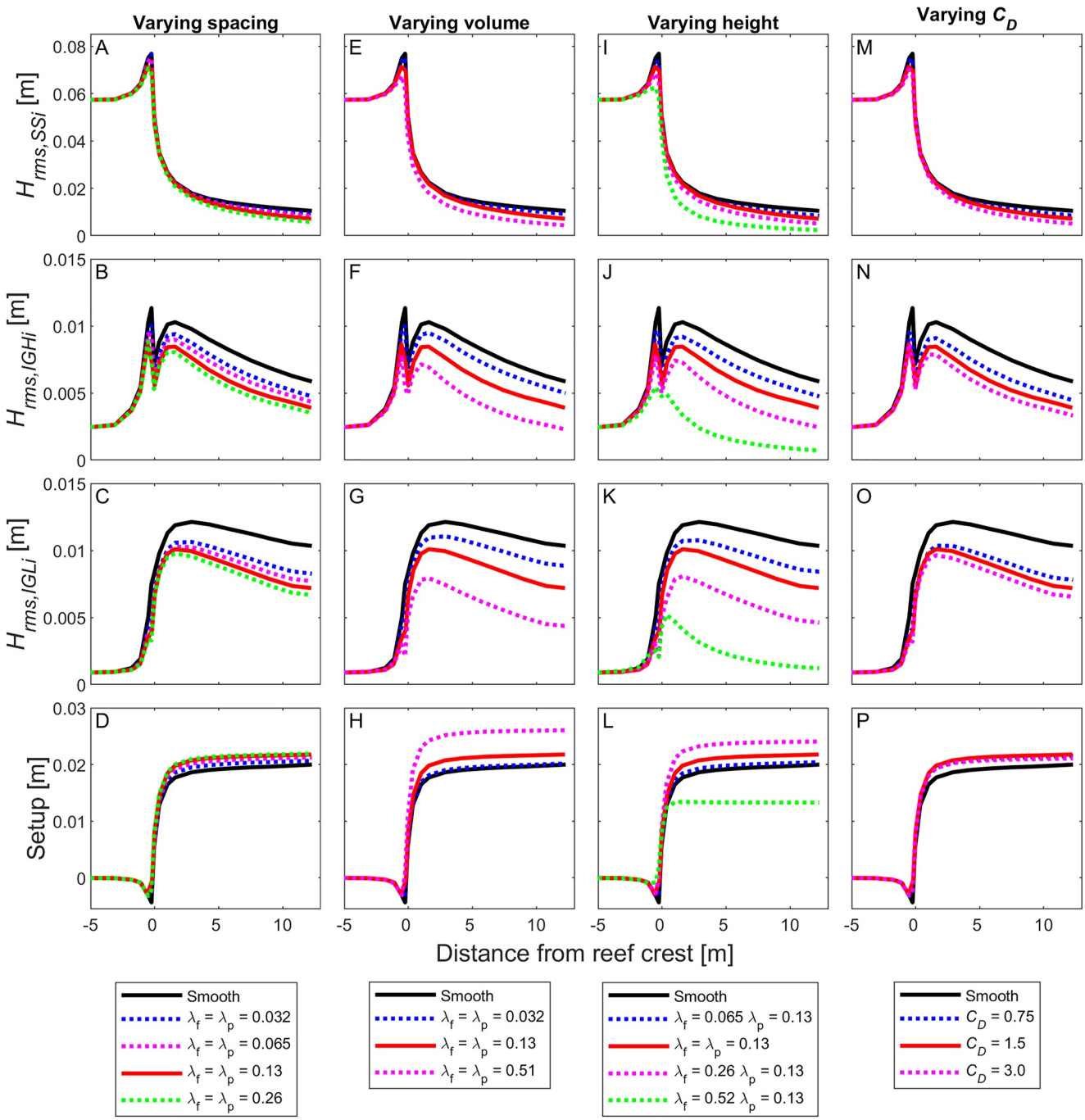

Figure 12. Incoming (top row) sea-swell ($H_{rms,SSi}$), (second row) high infragravity ($H_{rms,\ IGHi}$), and (third row) low infragravity ($H_{rms,\ IGLi}$) *rms* wave heights and (bottom row) wave setup predicted by SWASH with varying (first column) roughness spacing (smooth, 100, 200, 400, and 800 cubes/m^2), (second column) size (smooth, $l_w = l_l = h_c = 0.9$ cm, $l_w = l_l = h_c = 1.8$ cm, and $l_w = l_l = h_c = 3.6$ cm), (third column) roughness element heights (h_c) (smooth, 0.9, 3.6, and 7.2 cm), and (fourth column) drag coefficient (C_D). The dimensions and density of the roughness elements are used to calculate, via Equation 5, the frontal area of roughness elements per unit plan area (λ_f) and the plan area of the roughness elements per unit plan area (λ_p). Solid curves are the parameters used in the laboratory study. The forcing conditions, fore-reef slope, reef flat length, and beach slope from Run 2 were used.

depths where the setup response is greater (Buckley et al., 2015; Svendsen, 1984). Increasing the fore-reef slope from 1/20 to 1/1 increased wave setup by 69% on the reef flat (x = 12.3 m), which increased the total reef flat water depths by 16%. The increased water depth allowed for larger depth-limited *SS* wave heights that were 31% larger on the reef flat for the 1/1 fore-reef slope compared to the 1/20 slope. The increase in incoming IG_H and

21699291, 2022, 11, Downloaded from https://agupubs.onlinelibrary.wiley.com/doi/10.1029/2022JC018857 by Technical University Delft, Wiley Online Library on [07/12/2022]. See the Terms and Conditions (https://onlinelibrary.wiley.com/terms-and-conditions) on Wiley Online Library for rules of use; OA articles are governed by the applicable Creative Commons License

21699291, 2022, 11, Downloaded from https://agupubs.onlinelibrary.wiley.com/doi/10.1029/2022JC018857 by Technical University Delft, Wiley Online Library on [07/12/2022]. See the Terms and Conditions (https://onlinelibrary.wiley.com/terms-and-conditions) on Wiley Online Library for rules of use; OA articles are governed by the applicable Creative Commons License

IG_L waves on the reef flat was even larger: 56% for IG_H and 82% for IG_L. This is likely due to the relative efficiency of the breakpoint forcing mechanism of *IG* wave generations over free long wave generation by bound wave release on steep slopes like coral fore-reef slopes (Buckley et al., 2018a; Péquignet et al., 2009; Pomeroy et al., 2012). Like wave setup, the efficiency of the breakpoint forcing mechanism is greater for steeper slopes (Becker et al., 2016).

In contrast to the obvious impact of the fore-reef slope on wave dynamics and wave setup, the slope of reef-fronted beaches had a more subtle influence for these shallow reef cases. This is because unlike open coast beaches, on shallow reefs the primary surf zone is on the fore-reef slope separated from the shoreline by a reef flat or lagoon. The waves that reach the beach are typically much smaller and have a longer period than the incident waves that break on the fore-reef slope and reef crest (Figures 2–4) (Becker et al., 2016; Cheriton et al., 2016; Péquignet et al., 2009; Pomeroy et al., 2012). Thus, waves have lower steepness (i.e., wave height divided by wave length), and locally calculated Iribarren numbers are significantly higher than those calculated based on the offshore incident wave conditions (Cheriton et al., 2016). As a result, the transition from reflective to breaking occurs at a much milder beach slope than typical of open coast beaches due to the low steepness landward of the reef surf zone. This is somewhat analogous to observations of wave interactions with dikes fronted by a shallow foreshore, which have shown that the waves reaching the beach toe and swash zone are significantly longer period than the incident *SS* waves and therefore interact differently with the beach slope (Lashley et al., 2020; van Gent, 2001). However, these dynamics change when the still water depth over the reef flat becomes greater than the offshore significant wave height (Figure 10).

For smaller waves and/or deeper reefs ($h_{0,r}/H_{rms,0} > 1$) than considered by Buckley et al. (2016), wave breaking may be reduced or absent on the fore-reef with the primary surf zone occurring at the reef-fronted beach (Figure 10). These deeper cases are also relevant to higher still water level conditions that may occur due to large tides, storm surge, or sea-level rise and coral degradation. The swash and wave setup components of runup varied in their responses to increased still water levels resulting in a mixed trend in the total runup. Due to decreased wave breaking dissipation on the fore-reef, the swash component of runup increased with increased still water level until a maximum value was reached when wave breaking on the fore-reef ceased when $h_{0,r}$ was greater than four times $H_{rms,0}$. At these high water levels, wave setup on the reef flat was near zero, but wave setup generated due to wave breaking on the beach reached a maximum. Given that the shoreline wave setup is the sum of wave setup generated on the reef profile and the beach, it showed a parabolic response with a minimum at $h_{0,r}$ equal to $H_{rms,0}$. Thus the total 2% exceedance wave runup, decreased slightly with increased $h_{0,r}$ before reaching a maximum when $h_{0,r}$ was greater than four times $H_{rms,0.}$

Resonant amplification of IG_L waves is a major concern on reef-lined coasts and is thought to be related to the wave group forcing frequencies relative to the natural mode of the reef flat, damping by frictional dissipation on the reef flat, and beach slope (Becker et al., 2016; Buckley et al., 2018a; Péquignet et al., 2009; Roeber & Bricker, 2015). Based on these criteria, the smooth reef simulations should have the most ideal conditions for resonant amplification and indeed evidence of resonant amplification was found by Buckley et al. (2018a). However, without numerical modeling, Buckley et al. (2018a) lacked a method to quantify the amount of resonant amplification as incoming IG_L wave heights on the reef flat before resonant amplification were unknown from the experimental results. Here, the validated numerical model allows further investigation. A mild 1/400 slope beach was used in the lee of the reef to dissipate incoming waves including IG_L at the shoreline well maintaining similar *SS* wave dynamics and wave setup (Figure 7). With the forcing conditions from Run 2, the IG_L reflection coefficient on the reef flat ($x = 12.3$ m) was 0.18 for the 1/400 beach slope compared to 0.98 for the steeper 1/12 beach slope (Figure 7). With the 1/400 beach slope, the possibility of resonant amplification is thus greatly reduced as there is significantly less outgoing IG_L wave energy available to be trapped on the reef flat, which is a requirement for resonant amplification (Roeber & Bricker, 2015). Therefore, if resonant amplification significantly increased the incoming reef flat wave heights in the laboratory data with the 1/12 beach slope, a significant reduction in incoming *rms* wave height would be expected with the beach slope change. However, there was little observed change in incoming *rms* wave heights on the reef flat (Figures 7 C and 8), indicating resonant amplification was not significantly affecting the bulk incoming *rms* wave heights despite the observations of increased energy at the resonant frequencies of the reef (Figure 4; Buckley et al., 2018a). Wave runup was typically greater for steeper beach slope cases (Figure 9), but that is not indicative of resonant amplification due to the well-known dependence of wave runup on beach slope (van Gent, 2001). Separate tests were performed comparing wave runup on a profile consisting of only the reef flat and a 1/12 beach slope (not shown). Simulations were forced with either

21699291, 2022, 11, Downloaded from https://agupubs.onlinelibrary.wiley.com/doi/10.1029/2022JC018857 by Technical University Delft, Wiley Online Library on [07/12/2022]. See the Terms and Conditions (https://onlinelibrary.wiley.com/terms-and-conditions) on Wiley Online Library for rules of use; OA articles are governed by the applicable Creative Commons License

reef flat observations from the previous reef fronted 1/12 or 1/400 beach slope simulations. As with incoming *rms* wave heights, these simulations showed comparable wave runup regardless of the beach slope from which the forcing was derived.

In addition to the characteristics of individual reefs, the coastal protection utility of reefs versus open coast beaches is highly dependent on the open coast beach case that the reef case is compared to. For example, for a reef with a 1/5 fore-reef slope fronting a beach with a mild beach slope ($\beta < \sim 1/30$; Figure 9a), the wave runup can be larger than for a plane beach of the same slope. In contrast, normalized wave runup was up to three times larger for plane beaches lacking a reef for steeper beach slopes ($\beta > \sim 1/30$; Figure 9a). For mild beach slopes, the swash component of wave runup is limited for all cases (open coast beach and reef) due to wave breaking and saturation of the swash spectrum (Figure 9b) (Huntley et al., 1977). However, wave setup generation is greater for the reef cases due to more intense wave breaking (larger radiation stress gradients) in shallower water depths on the steep fore-reef and shallow reef flat than occurs on the mild slope plane beaches (Figure 9c) (Battjes, 1974a, 1974b). Increasing the beach slope on open coast beaches increases the wave frequency where waves of a given height transition from reflecting at lower frequencies to breaking at higher frequencies (Guza et al., 1984; Hedges & Mase, 2004; Huntley et al., 1977). This results in a rapid increase in the swash component of wave runup (Figure 9b). On the reef profile at the beach toe, a large portion of the wave energy is in *IG* frequencies (Figure 4) that are typically reflective except at very mild beach slopes where breaking can occur (de Bakker et al., 2014; van Dongeren et al., 2007). This results in less wave runup response to beach slope for the reef-fronted beaches than the plane beaches (Figure 9b).

4.2. Influence of Reef Roughness Characteristics and Distribution

Reef roughness enhances the coastal protection provided by reefs (Figure 9). The transition from negative to positive coastal protection utility of the reef structure is also shifted with the introduction of roughness (Figure 9). While the laboratory experiments of Buckley et al. (2018a) only considered uniformly smooth or rough reefs, reefs generally have natural spatial heterogeneity in coral cover and rugosity between reef zones (reef crest, slope, flat) that can be tested with the numerical model. This variability in roughness is due to factors such as variation in physical processes, light availability, and temperature, with the lowest coral cover typically found in reef flat environments (Graham et al., 2014). For degraded reefs, spatial variability in roughness is also expected due to spatially inhomogeneous coral degradation caused; for example, by coral bleaching, water quality issues, and cyclone damage that can impact different zones of a reef (Lowe & Falter, 2015). Our results suggest the most coastal protection utility is generated by a uniformly rough reef (17% decrease in wave runup from smooth) followed by a smooth reef slope and rough reef flat (11% decrease from smooth), and a rough reef slope and smooth reef flat (6% decrease from smooth) (Figure 12). As the lowest coral cover is typically found in reef flat environments (Graham et al., 2014), they may provide less protection than uniformly rough reefs and would be a key area for enhancing roughness through either coastal protection structures or coral restoration.

The numerical model also allows for the testing of the abundance (density), volume, height, and assigned drag coefficient (C_D) of roughness elements (Figure 13). Increasing the abundance of roughness elements was found to have a diminishing return above 100 elements/m^2. Increasing the volume of roughness elements increased rates of wave dissipation, but also increased wave setup. Increasing C_D had little effect on wave setup but reduced wave dissipation.

Of the different roughness properties, our simulations show wave runup was most sensitive to roughness height (Figure 13). Even when controlling for the volume and frontal area of roughness elements (not shown), roughness element height had the strongest influence on the hydrodynamics and subsequent wave runup. This is not surprising as wave velocities are generally larger near the surface. Increasing the height of roughness elements also decreased the relative submergence on the reef flat $h_c/(h_0 + \overline{\eta})$, which contributes to driving greater flow through the canopy (McDonald et al., 2006; Rosman & Hench, 2011). In contrast to varying other parameters, roughness height can be increased without significantly diverting flow over the canopy as flow over the canopy is limited by decreasing the relative submergence of roughness elements and the increased pressure gradient (Nepf & Vivoni, 2000). However, increasing the height of roughness elements results in slightly increased wave setup, except for the case of the tallest roughness elements (which were emergent). For emergent roughness elements, a significant reduction in setup was observed. This was likely due to onshore-directed mean drag forces in the wave

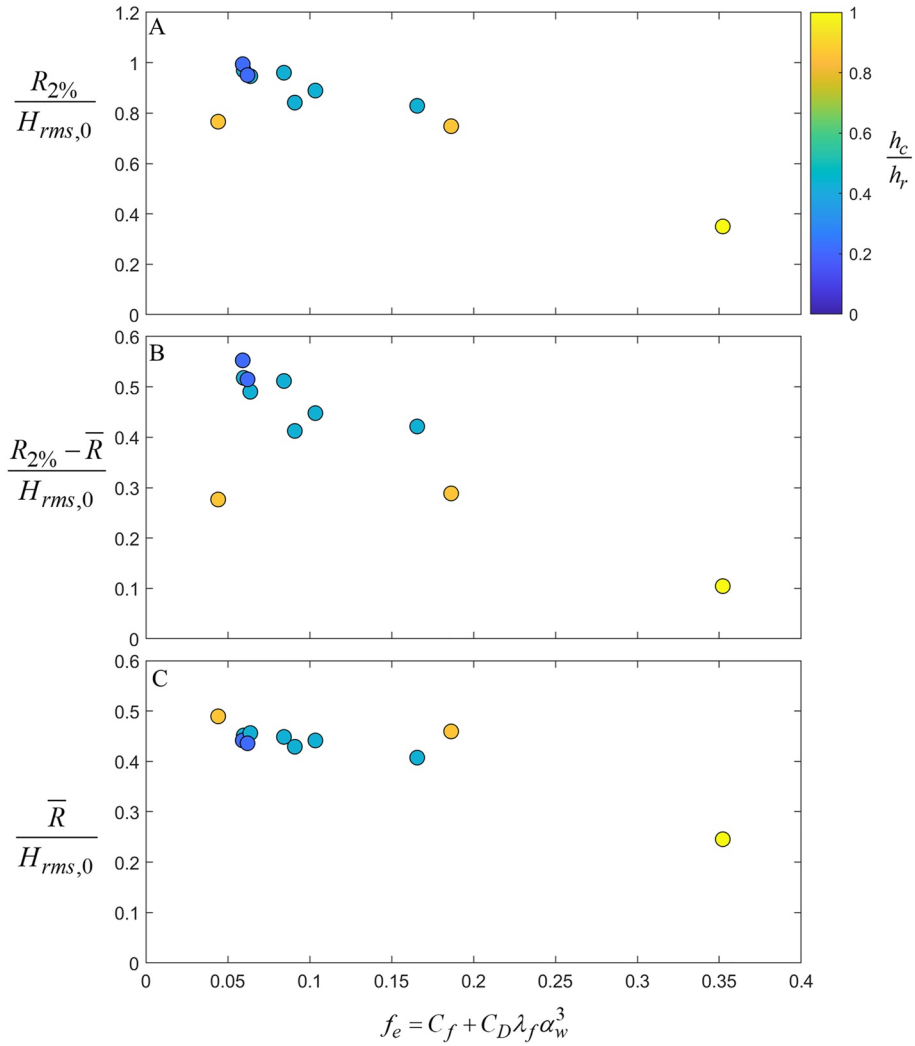

Figure 13. The 2% exceedance wave runup (a, b) 2% exceedance swash, and (c) wave setup at the shoreline with each normalized by deep water *rms* wave height versus wave energy dissipation factor f_e calculated following Lowe et al. (2007) using canopy geometry. In the calculation, the incident peak wave period is used and a *rms* velocity of 0.1 m/s is assumed based on observations near the reef crest. The colormap gives the relative submergence of roughness elements on the reef flat for still water level conditions. The forcing conditions, fore-reef slope, reef flat length, and beach slope from Run 2 were used.

crests (Dean & Bender, 2006). Results from the numerical model used here suggest that restoration strategies that increase roughness height on the reef flat will most efficiently reduce wave runup and therefore coastal hazard risk. However, there would be an increased risk of damage to tall and sparse roughness elements due to larger drag forces predicted by the numerical model (Storlazzi et al., 2005). For example, this would require using more robust corals or substrate in a restoration project.

4.3. Quantifying the Impact of Roughness on Wave Runup

Reef restoration projects seek to enhance coral cover by transferring corals or providing hard substrate for corals to colonize (Chavanich et al., 2015). An additional benefit of these restoration projects may be an increase in coastal protection (Ferrario et al., 2014; Reguero et al., 2018), yet there is limited research on the design optimization of such strategies to reduce hazard risk and increase the resilience of vulnerable coastal communities. Predictive capability to estimate runup at the shoreline adjacent to a reef relies on the development of an expression to capture the complex roughness characteristics and dissipation processes. Here we test the extent to which the

21699291, 2022, 11, Downloaded from https://agupubs.onlinelibrary.wiley.com/doi/10.1029/2022JC018857 by Technical University Delft, Wiley Online Library on [07/12/2022]. See the Terms and Conditions (https://onlinelibrary.wiley.com/terms-and-conditions) on Wiley Online Library for rules of use; OA articles are governed by the applicable Creative Commons License

dissipation factor proposed by Lowe et al. (2007) encapsulates the impact of reef roughness on wave dissipation and hence $R_{2\%}$ for the simulations presented in Figure 12. Lowe et al. (2007) give the wave dissipation factor as:

$$f_e = C_f + C_D \lambda_f \alpha_w^3 \tag{8}$$

where α_w is an attenuation parameter calculated as the ratio of the in-canopy *rms* flow velocity to the above-canopy *rms* flow velocity. The attenuation parameter, α_w, is calculated here assuming monochromatic waves of period $T_p = 2.26$ s and an above-canopy *rms* flow velocity of 0.1 m/s, which is representative of flow measured on the fore-reef near the reef crest. We note that Equation 8 is only used to give an approximate estimate of the effect changes to roughness will have on wave dissipation, as the *rms* flow velocities and wave spectra change rapidly through the surf zone (Figures 2 and 3). Despite this limitation, f_e does provide a useful indication how wave runup and particularly its swash component will respond to roughness (Figure 13). In addition to the trend of decreasing wave runup with f_e there is also a dependence on relative submergence $h_c/(h_0 + \overline{\eta})$ not fully captured by the model of Lowe et al. (2007), which assumes small $h_c/(h_0 + \overline{\eta})$ (Figure 13). Increasing $h_c/(h_0 + \overline{\eta})$ directs more flow through the canopy (McDonald et al., 2006; Rosman & Hench, 2011), which increases drag forces and reduces the $R_{2\%}$. As such, f_e and $h_c/(h_0 + \overline{\eta})$ can both be considered as parameters that contribute to wave runup reduction.

4.4. Limitations of This Study and Further Work

This study focused on 1D reef profiles and is therefore most representative of reefs, which can be considered along-shore uniform with no significant channels or discontinuities in the along-shore extent of the reef crest. This limitation ensured that the numerical study was consistent with the laboratory study undertaken by Buckley et al. (2016). However, many natural reefs have channels through the reef crest that facilitate the circulation of water from the reef to the channels and then offshore (Clark et al., 2020; Lindhart et al., 2021; Lowe et al., 2009b; Rijnsdorp et al., 2021). This circulation pattern has been shown to reduce wave setup at the shoreline (Lowe et al., 2009b; Rijnsdorp et al., 2021). Consequently, it would be reasonable to argue that such 2D effects are likely to result in a significant reduction in the extent of coastal flooding behind reefs with large channels, as wave setup was consistently found in this study to be a large component of $R_{2\%}$ (Figures 5 and 9). This was recently confirmed in a laboratory experiment using a 2D reef morphology (Yao, Chen, et al., 2020; Zheng et al., 2020).

For the along-shore uniform reefs used in this study, wave setup slightly increases with the number and size of roughness elements (Figure 12) due to increased offshore-directed time-averaged bottom drag forces (Buckley et al., 2016). This effect limits some of the coastal protection advantages of having a denser canopy for reefs where the reef bathymetry is approximately alongshore uniform (as in the present study). However, for barrier reefs and fringing reefs with channels bisecting the reef crest, wave setup at the shoreline is expected to be reduced to some extent with the introduction of roughness on the reef flat, as mean near-bed velocities and, hence, time-averaged bottom drag forces are directed onshore (Clark et al., 2020; Lindhart et al., 2021; Lowe et al., 2009b; Rijnsdorp et al., 2021; Yao et al., 2018; Zheng et al., 2020).

The waves used in this study were incident to the reef profile with no directional spreading. Increased directional spreading has been found to reduce $R_{2\%}$ on beach profiles (Guza & Feddersen, 2012). However, the extent to which directional spreading reduced $R_{2\%}$ for reefs remains unclear, as the hydrodynamics at the shoreline is to some extent decoupled from the incident waves due to the narrow wave-breaking zone that is often located some distance from the shoreline. Irrespective of the impact of directional spreading, the results of this study are likely to be a worst-case assessment of the extent of runup that may be expected behind reefs due to the along-shore uniform reef used here. Nevertheless, the results are expected to be representative of many fringing reefs including the relative changes to wave runup with reef and beach slope and roughness.

We also note that extreme runup statistics are inherently uncertain due to irregular waves and the small number of runup maxima used to compute extreme statistics (Liu et al., 2021; Rutten et al., 2021). This inherent uncertainty may lead to some erroneous results when comparing small differences in extreme runup between individual runs. However, the overall results presented here rely on trends over several runs and are therefore less susceptible to aleatoric uncertainty. However, future studies may benefit from ensemble averaging of the same runs with different random phases of the wave components.

21699291, 2022, 11, Downloaded from https://agupubs.onlinelibrary.wiley.com/doi/10.1029/2022JC018857 by Technical University Delft, Wiley Online Library on [07/12/2022]. See the Terms and Conditions (https://onlinelibrary.wiley.com/terms-and-conditions) on Wiley Online Library for rules of use; OA articles are governed by the applicable Creative Commons License

21699291, 2022, 11, Downloaded from https://agupubs.onlinelibrary.wiley.com/doi/10.1029/2022JC018857 by Technical University Delft, Wiley Online Library on [07/12/2022]. See the Terms and Conditions (https://onlinelibrary.wiley.com/terms-and-conditions) on Wiley Online Library for rules of use; OA articles are governed by the applicable Creative Commons License

5. Conclusions

Laboratory flume experiments and a phase-resolving wave-flow model were used to investigate the wave-driven water levels in the lee of fringing reefs. The validated numerical model was then used to assess the effect of varying reef geometry and roughness characteristics. The numerical model, which included a parametrization of the time-varying drag forces generated by roughness elements, reproduced laboratory observations of waves and runup over both smooth and rough fringing reefs. The numerical model was then used to assess the coastal protection utility of coral reefs with varying morphologies and roughness. The coastal protection utility of reefs was found to be heavily dependent on the properties of the reef and shoreline, wave and water level conditions, and most importantly what the reef is being compared to. In this study, beach slope was found to be of key importance with mild slope beaches having higher runup and wave setup when fronted by a shallow reef (Figure 9). This is due to the high wave setup generated on the fore-reef surf zone (Figures 2 and 3) compared to the mild slope plane beach lacking a reef (Figure 9c). For our examples, a beach slope of ~1/30 was the transition from negative to positive coastal protection utility of the reef, suggesting that beach slope can have as large of an influence on runup as whether a reef is present or not. However, large reductions in wave runup are possible with the rough reef profile reducing wave runup by 72% (67% for the smooth reef) compared to an open-coast site with a beach slope of 1/2.

The loss of coral cover has the potential to reduce some of the coastal protection utility of reefs as coral reef degradation will likely affect the distribution, size, shape, and abundance of corals (Perry et al., 2018). Our study demonstrates that this will have important impacts on the wave and setup height, which are key components of shoreline runup. Many reef restoration projects seek to enhance coral cover by transferring corals or providing hard substrate for corals to colonize (Chavanich et al., 2015). An additional benefit of these restoration projects may be an increase in coastal protection (Ferrario et al., 2014; Reguero et al., 2018), and numerical models such as SWASH, which include roughness, will be key to design optimization. This is becoming increasingly important as attention is placed on how best to put a monetary and socioeconomic value on coral reefs (Storlazzi et al., 2019; van Zanten et al., 2014), which ultimately may then be used to justify the funding of coral restoration projects (Narayan et al., 2016; Reguero et al., 2018). This study suggests that restoration strategies that increase roughness height on the reef flat using tall roughness elements most efficiently reduce wave runup and therefore coastal hazard risk.

Data Availability Statement

Data are hosted at the following location: https://www.sciencebase.gov/catalog/item/5a8f2aa8e4b06990605dddb6.

Acknowledgments
The experiment was funded by an ARC Future Fellowship Grant (FT110100201) and ARC Discovery Project Grant (DP140102026) to R.J.L. as well as a University of Western Australia Research Collaboration Award to R.J.L., M.L.B., A.W.P., and A.V.D. Additional funding was provided to A.V.D. by the "Hydro- and morphodynamics during extreme events" at Deltares (Project number 11200604). Any use of trade, firm, or product names is for descriptive purposes only and does not imply endorsement by the U.S. Government. The authors thank Tomohiro Suzuki for his correspondence while implementing the canopy flow model within SWASH. The authors thank Benjamin Norris and two anonymous reviews for reviewing and helping to improve this manuscript.

References

Alvarez-Filip, L., Dulvy, N. K., Gill, J. A., Cote, I. M., & Watkinson, A. R. (2009). Flattening of Caribbean coral reefs: Region-wide declines in architectural complexity. *Proceedings of the Royal Society B: Biological Sciences*, *276*, 3019–3025. https://doi.org/10.1098/rspb.2009.0339

Baldock, T. E., Golshani, A., Callaghan, D. P., Saunders, M. I., & Mumby, P. J. (2014). Impact of sea-level rise and coral mortality on the wave dynamics and wave forces on barrier reefs. *Marine Pollution Bulletin*, *83*, 155–164. https://doi.org/10.1016/j.marpolbul.2014.03.058

Battjes, J. A. (1974a). Computation of set-up, longshore currents, run-up and overtopping due to wind-generated waves.

Battjes, J. A. (1974b). Surf similarity. *Coastal Engineering Proceedings*, *1*, 26. https://doi.org/10.1061/9780872621138.029

Becker, J. M., Merrifield, M. A., & Yoon, H. (2016). Infragravity waves on fringing reefs in the tropical Pacific: Dynamic setup. *Journal of Geophysical Research: Oceans*, *121*, 3010–3028. https://doi.org/10.1002/2015jc011516

Bouws, E., Gunther, H., Rosenthal, W., & Vincent, C. L., (1985). Similarity of the wind wave spectrum in finite depth water. 1. Spectral form. *Journal of Geophysical Research*, *90*, 975–986. https://doi.org/10.1029/Jc090ic01p00975

Bowen, A. J., Inman, D. L., & Simmons, V. P. (1968). Wave set-down and set-up. *Journal of Geophysical Research*, *73*, 2569–2577. https://doi.org/10.1029/Jb073i008p02569

Buckley, M. L., Lowe, R. J., & Hansen, J. E. (2014). Evaluation of nearshore wave models in steep reef environments. *Ocean Dynamics*, *64*, 847–862. https://doi.org/10.1007/s10236-014-0713-x

Buckley, M. L., Lowe, R. J., Hansen, J. E., & Van Dongeren, A. R. (2015). Dynamics of wave setup over a steeply-sloping fringing reef. *Journal of Physical Oceanography*, *45*, 3005–3023. https://doi.org/10.1175/JPO-D-15-0067.1

Buckley, M. L., Lowe, R. J., Hansen, J. E., & Van Dongeren, A. R. (2016). Wave setup over a fringing reef with large bottom roughness. *Journal of Physical Oceanography*, *46*, 2317–2333. https://doi.org/10.1175/Jpo-D-15-0148.1

Buckley, M. L., Lowe, R. J., Hansen, J. E., van Dongeren, A. R., & Storlazzi, C. D. (2018a). Mechanisms of wave-driven water level variability on reef-fringed coastlines. *Journal of Geophysical Research: Oceans*, *123*, 3811–3831. https://doi.org/10.1029/2018jc013933

Buckley, M. L., Lowe, R. J., Hansen, J. E., van Dongeren, A. R., & Storlazzi, C. D. (2018b). *Water level and velocity measurements from the 2012 University of Western Australia Fringing Reef Experiment (UWAFRE)*. U.S. Geological Survey data release. https://doi.org/10.5066/F71V5D7J

Carrier, G. F., & Greenspan, H. P. (1958). Water waves of finite amplitude on a sloping beach. *Journal of Fluid Mechanics*, *4*, 97–109. https://doi.org/10.1017/S0022112058000331

Chavanich, S., Soong, K., Zvuloni, A., Rinkevich, B., & Alino, P. (2015). Conservation, management, and restoration of coral reefs. *Zoology*, *118*, 132–134. https://doi.org/10.1016/j.zool.2015.01.002

Cheriton, O. M., Storlazzi, C. D., & Rosenberger, K. J. (2016). Observations of wave transformation over a fringing coral reef and the importance of low-frequency waves and offshore water levels to runup, overwash, and coastal flooding. *Journal of Geophysical Research: Oceans*, *121*, 3121–3140. https://doi.org/10.1002/2015jc011231

Clark, S. J., Becker, J. M., Merrifield, M. A., & Behrens, J. (2020). The influence of a cross-reef channel on the wave-driven setup and circulation at Ipan, Guam. *Journal of Geophysical Research: Oceans*, *125*(7), e2019JC015722. https://doi.org/10.1029/2019JC015722

de Bakker, A. T. M., Tissier, M. F. S., & Ruessink, B. G. (2014). Shoreline dissipation of infragravity waves. *Continental Shelf Research*, *72*, 73–82. https://doi.org/10.1016/j.csr.2013.11.013

Demirbilek, Z., Nwogu, O. G., Ward, D. L., & Sánchez, A. (2009). Wave transformation over reefs: Evaluation of one-dimensional numerical models. *Coastal and Hydraulics Laboratory. Model Evaluation Report.*

Falter, J. L., Atkinson, M. J., & Merrifield, M. A. (2004). Mass transfer limitation of nutrient uptake by a wave-dominated reef flat community. *Limnology & Oceanography*, *49*, 1820–1831. https://doi.org/10.4319/lo.2004.49.5.1820

Falter, J. L., Lowe, R. J., Zhang, Z. L., & McCulloch, M. (2013). Physical and biological controls on the carbonate chemistry of coral reef waters: Effects of metabolism, wave forcing, sea level, and geomorphology. *PLoS One*, *8*, e53303. https://doi.org/10.1371/journal.pone.0053303

Ferrario, F., Beck, M. W., Storlazzi, C. D., Micheli, F., Shepard, C. C., & Airoldi, L. (2014). The effectiveness of coral reefs for coastal hazard risk reduction and adaptation. *Nature Communications*, *5*. 3794. https://doi.org/10.1038/ncomms4794

Filipot, J.-F., & Cheung, K. F. (2012). Spectral wave modeling in fringing reef environments. *Coastal Engineering*, *67*, 67–79. https://doi.org/10.1016/j.coastaleng.2012.04.005

Franklin, G. L., & Torres-Freyermuth, A. (2022). On the runup parameterisation for reef-lined coasts. *Ocean Modelling*, *169*, 101929. https://doi.org/10.1016/j.ocemod.2021.101929

Gawehn, M., van Dongeren, A., van Rooijen, A., Storlazzi, C. D., Cheriton, O. M., & Reniers, A. (2016). Identification and classification of very low frequency waves on a coral reef flat. *Journal of Geophysical Research: Oceans*, *121*, 7560–7574. https://doi.org/10.1002/2016jc011834

Graham, N. A. J., Chong-Seng, K. M., Huchery, C., Januchowski-Hartley, F. A., & Nash, K. L. (2014). Coral reef community composition in the context of disturbance history on the Great Barrier Reef, Australia. *PLOS ONE*, *9*(7), e101204. https://doi.org/10.1371/journal.pone.0101204

Guza, R. T., & Feddersen, F. (2012). Effect of wave frequency and directional spread on shoreline runup. *Geophysical Research Letters*, *39*. https://doi.org/10.1029/2012gl051959

Guza, R. T., Thornton, E. B., & Holman, R. A. (1984). Swash on steep and shallow beaches. *Coastal Engineering*, *1984*, 708–723. https://doi.org/10.9753/icce.v19.48

Hansen, J. E., Raubenheimer, B., List, J. H., & Elgar, S. (2015). Modeled alongshore circulation and force balances onshore of a submarine canyon. *Journal of Geophysical Research: Oceans*, *120*, 1887–1903. https://doi.org/10.1002/2014jc010555

Harris, D. L., Rovere, A., Casella, E., Power, H., Canavesio, R., Collin, A., et al. (2018). Coral reef structural complexity provides important coastal protection from waves under rising sea levels. *Science Advances*, *4*, eaao4350. https://doi.org/10.1126/sciadv.aao4350

Hedges, T. S., & Mase, H. (2004). Modified Hunt's equation incorporating wave setup. *Journal of Waterway, Port, Coastal, and Ocean Engineering*, *130*, 109–113. https://doi.org/10.1061/(asce)0733-950x(2004)130:3(109)

Huntley, D. A., Guza, R. T., & Bowen, A. J. (1977). A universal form for shoreline run-up spectra? *Journal of Geophysical Research*, *82*, 2577–2581. https://doi.org/10.1029/JC082i018p02577

Jadhav, R. S., Chen, Q., & Smith, J. M. (2013). Spectral distribution of wave energy dissipation by salt marsh vegetation. *Coastal Engineering*, *77*, 99–107. https://doi.org/10.1016/j.coastaleng.2013.02.013

Lashley, C. H., Roelvink, D., van Dongeren, A., Buckley, M. L., & Lowe, R. J. (2018). Nonhydrostatic and surfbeat model predictions of extreme wave run-up in fringing reef environments. *Coastal Engineering*, *137*, 11–27. https://doi.org/10.1016/j.coastaleng.2018.03.007

Launder, B. E., & Spalding, D. B. (1974). The numerical computation of turbulent flows. *Computer Methods in Applied Mechanics and Engineering*, *3*(2), 269–289. https://doi.org/10.1016/0045-7825(74)90029-2

Lentz, S. J., Churchill, J. H., Davis, K. A., & Farrar, J. T. (2016). Surface gravity wave transformation across a platform coral reef in the Red Sea. *Journal of Geophysical Research: Oceans*, *121*, 693–705. https://doi.org/10.1002/2015jc011142

Lindhart, M., Rogers, J. S., Maticka, S. A., Woodson, C. B., & Monismith, S. G. (2021). Wave modulation of flows on open and closed reefs. *Journal of Geophysical Research: Oceans*, *126*, e2020JC016645. https://doi.org/10.1029/2020JC016645

Liu, Y., Liao, Z. L., Fang, K. Z., & Li, S. W. (2021). Uncertainty of wave runup prediction on coral reef-fringed coasts using SWASH model. *Ocean Engineering*, *242*, 110094. https://doi.org/10.1016/j.oceaneng.2021.110094

Lowe, R. J., Altomare, C., Buckley, M. L., da Silva, R. F., Hansen, J. E., Rijnsdorp, D., et al. (2022). Smoothed Particle Hydrodynamics simulations of reef surf zone processes driven by plunging irregular waves. *Ocean Modelling*, *171*, 101945. https://doi.org/10.1016/j.ocemod.2022.101945

Lowe, R. J., Buckley, M. L., Altomare, C., Rijnsdorp, D. P., Yao, Y., Suzuki, T., & Bricker, J. D. (2019). Numerical simulations of surf zone wave dynamics using smoothed particle hydrodynamics. *Ocean Modelling*, *144*, 101481. https://doi.org/10.1016/j.ocemod.2019.101481

Lowe, R. J., & Falter, J. L. (2015). Oceanic forcing of coral reefs. *Annual Review of Marine Science*, *7*, 43–66. https://doi.org/10.1146/annurev-marine-010814-015834

Lowe, R. J., Falter, J. L., Bandet, M. D., Pawlak, G., Atkinson, M. J., Monismith, S. G., & Koseff, J. R. (2005). Spectral wave dissipation over a barrier reef. *Journal of Geophysical Research*, *110*, C04001. https://doi.org/10.1029/2004jc002711

Lowe, R. J., Falter, J. L., Koseff, J. R., Monismith, S. G., & Atkinson, M. J. (2007). Spectral wave flow attenuation within submerged canopies: Implications for wave energy dissipation. *Journal of Geophysical Research*, *112*, C05018. https://doi.org/10.1029/2006jc003605

Lowe, R. J., Falter, J. L., Monismith, S. G., & Atkinson, M. J. (2009a). A numerical study of circulation in a coastal reef-lagoon system. *Journal of Geophysical Research*, *114*, C06022. https://doi.org/10.1029/2008jc005081

Lowe, R. J., Falter, J. L., Monismith, S. G., & Atkinson, M. J. (2009b). Wave-driven circulation of a coastal reef-lagoon system. *Journal of Physical Oceanography*, *39*, 873–893. https://doi.org/10.1175/2008jpo3958.1

Lowe, R. J., Koseff, J. R., & Monismith, S. G. (2005). Oscillatory flow through submerged canopies: 1. Velocity structure. *Journal of Geophysical Research*, *110*, C10016. https://doi.org/10.1029/2004jc002788

Lugo-Fernández, A., Roberts, H. H., Wiseman, W. J., Jr., & Carter, B. L. (1998). Water level and currents of tidal and infragravity periods at Tague Reef, St. Croix (USVI). *Coral Reefs*, *17*, 343–349. https://doi.org/10.1007/s003380050137

Ma, G. F., Su, S. F., Liu, S. G., & Chu, J. C. (2014). Numerical simulation of infragravity waves in fringing reefs using a shock-capturing non-hydrostatic model. *Ocean Engineering*, *85*, 54–64. https://doi.org/10.1016/j.oceaneng.2014.04.030

McDonald, C. B., Koseff, J. R., & Monismith, S. G. (2006). Effects of the depth to coral height ratio on drag coefficients for unidirectional flow over coral. *Limnology and Oceanography*, *51*(3), 1294–1301. https://doi.org/10.4319/lo.2006.51.3.1294

21699291, 2022, 11, Downloaded from https://agupubs.onlinelibrary.wiley.com/doi/10.1029/2022JC018857 by Technical University Delft, Wiley Online Library on [07/12/2022]. See the Terms and Conditions (https://onlinelibrary.wiley.com/terms-and-conditions) on Wiley Online Library for rules of use; OA articles are governed by the applicable Creative Commons License

Merrifield, M. A., Becker, J. M., Ford, M., & Yao, Y. (2014). Observations and estimates of wave-driven water level extremes at the Marshall Islands. *Geophysical Research Letters*, *41*, 7245–7253. https://doi.org/10.1002/2014gl061005

Monismith, S. G., Rogers, J. S., Koweek, D., & Dunbar, R. B. (2015). Frictional wave dissipation on a remarkably rough reef. *Geophysical Research Letters*, *42*, 4063–4071. https://doi.org/10.1002/2015gl063804

Munk, W. H., & Sargent, M. C. (1948). Adjustment of Bikini Atoll to ocean waves. *Eos, Transactions American Geophysical Union*, *29*, 855–860. https://doi.org/10.1029/TR029i006p00855

Murphy, A. H., (1988). Skill scores based on the mean-square error and their relationships to the correlation-coefficient. *Monthly Weather Review*, *116*, 2417–2425. https://doi.org/10.1175/1520-0493(1988)116<2417:ssbotm>2.0.co;2;2

Narayan, S., Beck, M. W., Reguero, B. G., Losada, I. J., van Wesenbeeck, B., Pontee, N., et al. (2016). The effectiveness, costs and coastal protection benefits of natural and nature-based defences. *PLoS One*, *11*, e0154735. https://doi.org/10.1371/journal.pone.0154735

Nelson, R. C., (1996). Hydraulic roughness of coral reef platforms. *Applied Ocean Research*, *18*, 265–274. https://doi.org/10.1016/S0141-1187(97)00006-0

Nepf, H. M., & Vivoni, E. R., (2000). Flow structure in depth-limited, vegetated flow. *Journal of Geophysical Research*, *105*, 28547–28557. https://doi.org/10.1029/2000jc900145

Pearson, S. G., Storlazzi, C. D., van Dongeren, A. R., Tissier, M. F. S., & Reniers, A. J. H. M. (2017). A Bayesian-based system to assess wave-driven flooding hazards on coral reef-lined coasts. *Journal of Geophysical Research: Oceans*, *122*, 10099–10117. https://doi.org/10.1002/2017jc013204

Péquignet, A. C. N., Becker, J. M., Merrifield, M. A., & Aucan, J. (2009). Forcing of resonant modes on a fringing reef during tropical storm Man-Yi. *Geophysical Research Letters*, *36*, L03607. https://doi.org/10.1029/2008gl036259

Perry, C. T., & Alvarez-Filip, L. (2019). Changing geo-ecological functions of coral reefs in the Anthropocene. *Functional Ecology*, *33*, 976–988. https://doi.org/10.1111/1365-2435.13247

Perry, C. T., Alvarez-Filip, L., Graham, N. A. J., Mumby, P. J., Wilson, S. K., & Kench, P. S. (2018). Loss of coral reef growth capacity to track future increases in sea level. *Nature*, *558*, 396–400. https://doi.org/10.1038/s41586-018-0194-z

Pomeroy, A., Lowe, R., Symonds, G., van Dongeren, A., & Moore, C. (2012). The dynamics of infragravity wave transformation over a fringing reef. *Journal of Geophysical Research*, *117*, C11022. https://doi.org/10.1029/2012jc008310

Quataert, E., Storlazzi, C., van Dongeren, A., & McCall, R. (2020). The importance of explicitly modelling sea-swell waves for runup on reef-lined coasts. *Coastal Engineering*, *160*, 103704. https://doi.org/10.1016/j.coastaleng.2020.103704

Quataert, E., Storlazzi, C., van Rooijen, A., Cheriton, O., & van Dongeren, A. (2015). The influence of coral reefs and climate change on wave-driven flooding of tropical coastlines. *Geophysical Research Letters*, *42*, 6407–6415. https://doi.org/10.1002/2015gl064861

Raichlen, F., & Hammack, J., Jr. (1975). Run-up due to breaking and non-breaking waves. *Coastal Engineering*, *1974*, 1937–1955.

Raubenheimer, B., & Guza, R. T., (1996). Observations and predictions of run-up. *Journal of Geophysical Research*, *101*, 25575–25587. https://doi.org/10.1029/96jc02432

Reguero, B. G., Beck, M. W., Agostini, V. N., Kramer, P., & Hancock, B. (2018). Coral reefs for coastal protection: A new methodological approach and engineering case study in Grenada. *Journal of Environmental Management*, *210*, 146–161. https://doi.org/10.1016/j.jenvman.2018.01.024

Rijnsdorp, D. P., Buckley, M. L., da Silva, R. F., Cuttler, M. V. W., Hansen, J. E., Lowe, R. J., et al. (2021). A numerical study of wave-driven mean flows and setup dynamics at a coral reef-lagoon system. *Journal of Geophysical Research: Oceans*, *126*, e2020JC016811. https://doi.org/10.1029/2020JC016811

Roeber, V., & Bricker, J. D. (2015). Destructive tsunami-like wave generated by surf beat over a coral reef during Typhoon Haiyan. *Nature Communications*, *6*, 7854. https://doi.org/10.1038/ncomms8854

Roeber, V., & Cheung, K. F. (2012). Boussinesq-type model for energetic breaking waves in fringing reef environments. *Coastal Engineering*, *70*, 1–20. https://doi.org/10.1016/j.coastaleng.2012.06.001

Roelvink, D., Reniers, A., van Dongeren, A., van Thiel de Vries, J., McCall, R., & Lescinski, J. (2009). Modelling storm impacts on beaches, dunes and barrier islands. *Coastal Engineering*, *56*, 1133–1152. https://doi.org/10.1016/j.coastaleng.2009.08.006

Rosman, J. H., & Hench, J. L. (2011). A framework for understanding drag parameterizations for coral reefs. *Journal of Geophysical Research-Oceans*, *116*, C08025. https://doi.org/10.1029/2010jc006892

Ruggiero, P., Holman, R. A., & Beach, R. A. (2004). Wave run-up on a high-energy dissipative beach. *Journal of Geophysical Research*, *109*, C06025. https://doi.org/10.1029/2003jc002160

Rutten, J., Torres-Freyermuth, A., & Puleo, J. A. (2021). Uncertainty in runup predictions on natural beaches using XBeach nonhydrostatic. *Coastal Engineering*, *166*, 103869. https://doi.org/10.1016/j.coastaleng.2021.103869

Sheppard, C., Dixon, D. J., Gourlay, M., Sheppard, A., & Payet, R. (2005). Coral mortality increases wave energy reaching shores protected by reef flats: Examples from the Seychelles. *Estuarine, Coastal and Shelf Science*, *64*, 223–234. https://doi.org/10.1016/j.ecss.2005.02.016

Shimozono, T., Tajima, Y., Kennedy, A. B., Nobuoka, H., Sasaki, J., & Sato, S. (2015). Combined infragravity wave and sea-swell runup over fringing reefs by super typhoon Haiyan. *Journal of Geophysical Research: Oceans*, *120*, 4463–4486. https://doi.org/10.1002/2015jc010760

Smit, P., Zijlema, M., & Stelling, G. (2013). Depth-induced wave breaking in a non-hydrostatic, near-shore wave model. *Coastal Engineering*, *76*, 1–16. https://doi.org/10.1016/j.coastaleng.2013.01.008

Stockdon, H. F., Holman, R. A., Howd, P. A., & Sallenger, A. H. (2006). Empirical parameterization of setup, swash, and runup. *Coastal Engineering*, *53*, 573–588. https://doi.org/10.1016/j.coastaleng.2005.12.005

Storlazzi, C. D., Brown, E. K., Field, M. E., Rodgers, K., & Jokiel, P. L. (2005). A model for wave control on coral breakage and species distribution in the Hawaiian Islands. *Coral Reefs*, *24*, 43–55. https://doi.org/10.1007/s00338-004-0430-x

Storlazzi, C. D., Gingerich, S. B., van Dongeren, A. p. R., Cheriton, O. M., Swarzenski, P. W., Quataert, E., et al. (2018). Most atolls will be uninhabitable by the mid-21st century because of sea-level rise exacerbating wave-driven flooding. *Science Advances*, *4*, eaap9741. https://doi.org/10.1126/sciadv.aap9741

Storlazzi, C. D., Reguero, B. G., Cole, A. D., Lowe, E., Shope, J. B., Shope, A. E., et al. (2019). Rigorously valuing the role of U.S. coral reefs in coastal hazard risk reduction. U.S. Geological Survey, (p. 52). https://doi.org/10.3133/ofr20191027

Suzuki, T., Hu, Z., Kumada, K., Phan, L. K., & Zijlema, M. (2019). Non-hydrostatic modeling of drag, inertia and porous effects in wave propagation over dense vegetation fields. *Coastal Engineering*, *149*, 49–64. https://doi.org/10.1016/j.coastaleng.2019.03.011

Svendsen, I. A., (1984). Wave heights and set-up in a surf zone. *Coastal Engineering*, *8*, 303–329. https://doi.org/10.1016/0378-3839(84)90028-0

Symonds, G., Huntley, D. A., & Bowen, A. J. (1982). Two-dimensional surf beat: Long wave generation by a time-varying breakpoint. *Journal of Geophysical Research*, *87*, 492–498. https://doi.org/10.1029/JC087iC01p00492

Torres-Garcia, L. M., Dalyander, P. S., Long, J. W., Zawada, D. G., Yates, K. K., Moore, C., & Olabarrieta, M. (2018). Hydrodynamics and sediment mobility processes over a degraded senile coral reef. *Journal of Geophysical Research: Oceans*, *123*, 7053–7066. https://doi.org/10.1029/2018jc013892

21699291, 2022, 11, Downloaded from https://agupubs.onlinelibrary.wiley.com/doi/10.1029/2022JC018857 by Technical University Delft, Wiley Online Library on [07/12/2022]. See the Terms and Conditions (https://onlinelibrary.wiley.com/terms-and-conditions) on Wiley Online Library for rules of use; OA articles are governed by the applicable Creative Commons License

van Dongeren, A., Battjes, J., Janssen, T., van Noorloos, J., Steenhauer, K., Steenbergen, G., & Reniers, A. (2007). Shoaling and shoreline dissipation of low-frequency waves. *Journal of Geophysical Research*, *112*, C02011. https://doi.org/10.1029/2006jc003701

van Dongeren, A., Klopman, G., Reniers, A., & Petit, H. (2002). High-quality laboratory wave generation for flumes and basins. *Ocean Wave Measurement And Analysis (2001)*, 1190–1199. https://doi.org/10.1061/40604(273)120

van Dongeren, A., Lowe, R., Pomeroy, A., Trang, D. M., Roelvink, D., Symonds, G., & Ranasinghe, R. (2013). Numerical modeling of low-frequency wave dynamics over a fringing coral reef. *Coastal Engineering*, *73*, 178–190. https://doi.org/10.1016/j.coastaleng.2012.11.004

van Gent, M. R. A., (2001). Wave runup on dikes with shallow foreshores. *Journal of Waterway, Port, Coastal, and Ocean Engineering*, *127*, 254–262. https://doi.org/10.1061/(asce)0733-950x(2001)127:5(254)(2001)127:5(254)

van Zanten, B. T., van Beukering, P. J. H., & Wagtendonk, A. J. (2014). Coastal protection by coral reefs: A framework for spatial assessment and economic valuation. *Ocean & Coastal Management*, *96*, 94–103. https://doi.org/10.1016/j.ocecoaman.2014.05.001

Yao, Y., Chen, S. G., Zheng, J. H., Zhang, Q. M., & Chen, S. B. (2020). Laboratory study on wave transformation and run-up in a 2DH reef-lagoon-channel system. *Ocean Engineering*, *215*, 107907. https://doi.org/10.1016/j.oceaneng.2020.107907

Yao, Y., Chen, X., Xu, C., Jia, M., & Jiang, C. (2021). Numerical modelling of wave transformation and runup over rough fringing reefs using VARANS equations. *Applied Ocean Research*, *118*, 102952. https://doi.org/10.1016/j.apor.2021.102952

Yao, Y., Huang, Z. H., He, W. R., & Monismith, S. G. (2018). Wave-induced setup and wave-driven current over Quasi-2DH reef-lagoon-channel systems. *Coastal Engineering*, *138*, 113–125. https://doi.org/10.1016/j.coastaleng.2018.04.009

Yao, Y., Huang, Z. H., Monismith, S. G., & Lo, E. Y. M. (2012). 1DH Boussinesq modeling of wave transformation over fringing reefs. *Ocean Engineering*, *47*, 30–42. https://doi.org/10.1016/j.oceaneng.2012.03.010

Yao, Y., Zhang, Q. M., Becker, J. M., & Merrifield, M. A. (2020). Boussinesq modeling of wave processes in field fringing reef environments. *Applied Ocean Research*, *95*, 102025. https://doi.org/10.1016/j.apor.2019.102025

Zheng, J. H., Yao, Y., Chen, S. G., Chen, S. B., & Zhang, Q. M. (2020). Laboratory study on wave-induced setup and wave-driven current in a 2DH reef-lagoon-channel system. *Coastal Engineering*, *162*, 103772. https://doi.org/10.1016/j.coastaleng.2020.103772

Zijlema, M., (2012). Modelling wave transformation across a fringing reef using SWASH. *Coastal Engineering Proceedings*, *1*(33), currents.26. https://doi.org/10.9753/icce.v33.currents.26

Zijlema, M., Stelling, G., & Smit, P. (2011). SWASH: An operational public domain code for simulating wave fields and rapidly varied flows in coastal waters. *Coastal Engineering*, *58*, 992–1012. https://doi.org/10.1016/j.coastaleng.2011.05.015

21699291, 2022, 11, Downloaded from https://agupubs.onlinelibrary.wiley.com/doi/10.1029/2022JC018857 by Technical University Delft, Wiley Online Library on [07/12/2022]. See the Terms and Conditions (https://onlinelibrary.wiley.com/terms-and-conditions) on Wiley Online Library for rules of use; OA articles are governed by the applicable Creative Commons License